Dielectric Behaviour of Insulating Papers Subjected to Mixed Electric Fields

Doctoral thesis
presented by

Ivan Semenov

born on 19.01.1991
citizen of the Russian Federation

submitted to
the Faculty of Electrical Engineering and
Information Technology
in Technische Universität Ilmenau
for the degree of Doctor of Engineering

First reviewer Prof. Dr.-Ing. habil. Jürgen Petzoldt
Second reviewer Prof. Dr. Christian Franck
Third reviewer Prof. Dr.-Ing. Carsten Leu

Day of submission: 14.08.2020
Day of defense: 12.05.2021

DOI: 10.22032/dbt.50393
URN: nbn:de:gbv:ilm1-2021000364

Abstract

The effect of the voltage waveform on dielectric properties of insulating materials utilised in power electronic converters is a question of practical importance that so far has not been thoroughly investigated. The electrical insulation of these devices can be subjected to a mixed electric field that consists of a multifrequency ac- and a high dc-component. Under the action of a mixed electric field of high intensity, field-dependent effects can occur in an insulating material. In some dielectrics the permittivity and loss factor can increase due to a high dc-field. Such effects cannot be elucidated with dielectric measurements employing either pure ac- or dc-voltage excitation. The present work discusses the influence of bias fields of up to 14 kV/mm on the complex permittivity of cellulosic insulating papers. Cellulose was selected as the object of study due to its unique properties of a natural polymer that allows the observation of ionic and dipolar relaxation mechanisms.

The work included the development of an experimental setup for measuring the complex permittivity of non-impregnated and oil-impregnated papers by means of an ac-voltage superimposed onto a high bias voltage. The influence of both ac- and dc-components of the mixed electric field were considered. Effects of the water content, temperature and the electrical contacting of the dielectric were described.

Earlier investigations of the effect of water on dielectric properties of cellulosic papers were confirmed within the present work. Ionic motions induced by the application of a high dc-field influenced the complex permittivity by occurring in its loss spectrum in form of a distinct relaxation peak. By examining the effect of the electrical contacting, it was concluded that, under the influence of very high local fields, the electrochemical decomposition of water caused the generation of free ions, i. e. protons. The appearance of a dielectric relaxation peak due to the proton motion was described with the model of random potential barriers. In dry papers, no effect of the bias field was found on the complex permittivity. The results suggest that the dipolar relaxation mechanisms due to the orientation of molecular groups of cellulose were unaffected by the application of an external bias field.

Impregnation with oil changed the dielectric behaviour of the paper. In the presence of water, the permittivity of the oil-impregnated paper increased upon the application of a bias field due to a space charge arising at boundaries of microscopic oil gaps between the electrode and the paper. In dry specimens, no changes in the permittivity caused by the bias field were found. An increase of the permittivity due to the interfacial polarisation was not observed at frequencies between 5 Hz and 1 MHz. It is suggested that in dry cellulose and oil, no non-linear effects due to bias fields of considered values take place.

Kurzfassung

Die Auswirkung der Spannungsform auf dielektrische Eigenschaften von Isolierstoffen, die in leistungselektronischen Umrichtern verwendet werden, ist eine Frage von praktischer Relevanz, die bisher nicht ausreichend untersucht ist. Die elektrische Isolation dieser Betriebsmittel kann einem elektrischen Mischfeld ausgesetzt werden, das aus einem mehrfrequenten Wechsel- und einem hohen Glecihanteil besteht. Durch die Wirkung eines hohen Mischfeldes ist das Auftreten feldabhängiger Effekte in einem Isoliermaterial möglich. In manchen Materialien kann es aufgrund eines hohen Gleichfeldes zur Erhöhung der Permittivität und des Verlustfaktors kommen. Solche Effekte können weder mit reinen Wechselspannungs- noch mit reinen Gleichspannungsmessungen aufgeklärt werden. In der vorliegenden Arbeit wird der Einfluss von Gleichfeldern von bis zu 14 kV/mm auf die komplexe Permittivität von zellulosebasierten Isolierpapieren untersucht. Die Zellulose eignet sich durch die einzigartigen Eigenschaften eines Naturpolymers, das die Beobachtung von ionischen und dipolaren Relaxationsmechanismen ermöglicht.

Die Untersuchungen basieren auf der Entwicklung experimenteller Aufbauten zur Messung der komplexen Permittivität mit einer hohen Mischspannung an nichtimprägnierten und ölimprägnierten Papierproben. Diese ermöglichen die Untersuchung des Einflusses sowohl der Wechsel- als auch der Gleichanteile des Mischfeldes. Effekte des Wassergehalts, der Temperatur und der elektrischen Kontaktierung des Isoliermaterials werden beschrieben.

Frühere Untersuchungen zum Einfluss des Wassers auf dielektrische Eigenschaften der Zellulosepapiere werden im Kontext der hier behandelten Spannungsbeanspruchung bestätigt. Die durch das Gleichfeld verursachte Bewegung der freien Ionen im feuchten nichtimprägnierten Papier ist mit Entstehung eines separaten Peaks im Verlustspektrum verbunden. Weiterführende experimentelle Untersuchungen zur elektrischen Kontaktierung verdeutlichen, dass unter dem Einfluss sehr hoher lokaler Felder die elektrochemische Zersetzung von Wasser die Erzeugung freier Ionen bewirkt, vor allem Protonen. Das Auftreten eines Verlustpeaks aufgrund der Protonenbewegung wird mit

dem Modell der zufälligen Potentialbarrieren beschrieben. Im trockenen Papier wird kein Einfluss des Gleichfeldes auf die komplexe Permittivität festgestellt. Dieses Ergebnis deutet darauf hin, dass die dipolaren Relaxationsmechanismen, die auf die Orientierung der Molekülgruppen der Zellulose zurückzuführen sind, beim Anlegen eines externen Gleichfeldes nicht beeinflusst werden.

Die Imprägnierung mit Öl verändert das dielektrische Verhalten des Papiers. In Anwesenheit von Wasser erhöht sich die Permittivität des ölimprägnierten Papiers beim Anlegen eines Gleichfeldes aufgrund der Raumladung, die an den Grenzen mikroskopischer Ölspalte zwischen der Elektrode und dem Papier entsteht. In getrockneten Proben werden keine Änderungen der Permittivität aufgrund des Gleichfeldes festgestellt. Eine Erhöhung der Permittivität, die als Folge der Grenzflächenpolarisation zu erwarten wäre, tritt in dem getrockneten Papier bei Frequenzen zwischen 5 Hz und 1 MHz nicht auf. Die Messergebnisse lassen erkennen, dass sowohl in der trockenen Zellulose als auch im trockenen Öl keine nichtlinearen Effekte durch das Anlegen eines hohen Gleichfeldes der betrachteten Feldstärke auftreten.

Erklärung

Ich versichere, dass ich die vorliegende Arbeit ohne unzulässige Hilfe Dritter und ohne Benutzung anderer als der angegebenen Hilfsmittel angefertigt habe. Die aus anderen Quellen direkt oder indirekt übernommenen Daten und Konzepte sind unter Angabe der Quelle gekennzeichnet.

Bei der Auswahl und Auswertung folgenden Materials haben mir die nachstehend aufgeführten Personen in der jeweils beschriebenen Weise unentgeltlich geholfen:

1. Dr. Carsten Leu (TU Ilmenau),
2. Dr. Andrea Knauer (TU Ilmenau) – Rasterelektronenmikroskopie.

Weitere Personen waren an der inhaltlich-materiellen Erstellung der vorliegenden Arbeit nicht beteiligt. Insbesondere habe ich hierfür nicht die entgeltliche Hilfe von Vermittlungs- bzw. Beratungsdiensten (Promotionsberater oder anderer Personen) in Anspruch genommen. Niemand hat von mir unmittelbar oder mittelbar geldwerte Leistungen für Arbeiten erhalten, die im Zusammenhang mit dem Inhalt der vorgelegten Dissertation stehen.

Die Arbeit wurde bisher weder im In- noch im Ausland in gleicher oder ähnlicher Form einer Prüfungsbehörde vorgelegt.

Ich bin darauf hingewiesen worden, dass die Unrichtigkeit der vorstehenden Erklärung als Täuschungsversuch bewertet wird und gemäß § 7 Abs. 10 der Promotionsordnung den Abbruch des Promotionsverfahrens zur Folge hat.

Ilmenau, 14.08.2020

Contents

1 Introduction

Owing to recent advancements in the power semiconductor technology, high voltage power devices based on wide-band-gap semiconductors with blocking voltages higher than 10 kV are in development.[1] As key components of isolated or non-isolated power electronic converters, these devices are intended to be utilised in medium voltage distribution and traction grids, thus substituting conventional low frequency transformers. An isolated power electronic converter known as "Solid-State Transformer" (SST)[2,3] or "Power Electronic Transformer"[4] is more flexible in the power flow control enabled by the pulse width modulation (PWM) and has a smaller volume and weight due to the increased operation frequency. The galvanic isolation of an SST is provided by a medium frequency transformer (MFT) operating at frequencies in the range of several kHz. The reduced volume of the transformer constitutes a higher power density that results in a higher operating temperature. Hence, the electrical insulation of an MFT, in contrast to low frequency power transformers, must safely function at elevated temperatures. The destructive effect of partial discharges at

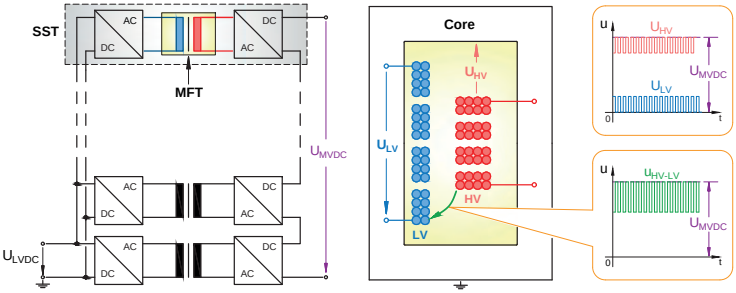

Figure 1.1: Schematic of the voltage acting on the insulation of the uppermost MFT of a solid-state transformer linking two dc-systems.

higher frequencies is another critical difference to low frequency applications. Ongoing research activities aim at the characterisation of insulating materials subjected to repetitive voltage pulses of high slew rates, high amplitudes and repetition frequency and their endurance under such conditions.[5–7] Major implications for the electrical insulation were found in inverter controlled motors employing PWM.[8]

Another advantage of an SST is the ease of configuring ac-ac, ac-dc or dc-dc interfaces. In ac-dc or dc-dc cascaded systems, besides a PWM-voltage, a dc-voltage of considerable intensity may be applied to the insulation of an MFT. Figure 1.1 schematically illustrates a dc-biased pulse voltage acting upon the insulation around the high voltage winding in the uppermost unit of cascaded SSTs. In literature, the electrical stress due to inverter voltages is often referred to as "mixed frequency" or "mixed voltage" stress. The term "mixed frequency voltage" describes a multifrequency voltage, whereas the term "mixed voltage" often denotes a single or multifrequency voltage superimposed onto a high dc-bias. According to this definition, the PWM-voltage in an SST is a mixed frequency voltage. In this work, the terms "mixed voltage" and "mixed field" denote a superposition of dc- and a single-frequency ac-component according to: $U(t) = U_{\mathrm{DC}} + U_{\mathrm{AC}} \sin(\omega t)$ and $E(t) = E_{\mathrm{DC}} + E_{\mathrm{AC}} \sin(\omega t)$.

The high harmonic content of the PWM voltage intensifies the dissipation of dielectric loss in the insulation of an MFT.[9–11] Thereby, the dielectric itself can become a heat source along with the magnetic core and windings. In the medium frequency range, dielectric losses in polymeric insulators in the glassy state are mostly associated with motions of permanent dipoles. Large-scale motions of polymer chains or charge carriers can add at higher temperatures. Depending on the insulating material, a simultaneous action of a high dc-voltage can alter the complex permittivity, provided the magnitude of the dc-field is

high enough to enter the non-linear region. In some dielectrics, the alteration of the complex permittivity may be associated with charge carrier motions at relatively low dc-fields. Therefore, the analysis of the effect of a high static field on the complex permittivity may be helpful in assessing insulating materials. A seemingly small increase of the permittivity within a wider range of frequencies could be an indication for a significant enhancement of the total dielectric loss under a multifrequency voltage excitation. In practice, the Joule heating due to the conduction current is much lower than the dielectric heating due to the alternating field stress.

The present work discusses the impact of a high static field on dielectric properties of cellulosic insulating papers. Oil-paper insulation that serves both insulating and cooling functions in oil-immersed transformers could be utilised in high power MFTs. A liquid dielectric enables a more efficient cooling of the active part compared to solid insulation with a lower thermal conductivity. Impregnated fibrous materials enhance the electrical strength of the insulation and act as a mechanical support for the transformer core and windings. Synthetic fibrous materials with superior characteristics than cellulosic papers are available. However, the advantage of cellulosic papers is a relatively simple manufacturing process requiring cheap raw materials. At the same time, their main drawback is a lower thermal stability in comparison to high-temperature synthetic fibres and a pronounced hydrophilicity that negatively affects the dielectric properties. So far, no fundamental research has been carried out on cellulosic materials under the aspect of their application in power electronic converters.

1.1 Effect of a High DC-Field

In what follows, a brief account of the influence of a high static field on dielectric properties of typical insulating materials is given. At

moderate intensities of the static field, the polarisation of the dielectric is in a linear dependence with the electric field $\boldsymbol{P} = \chi \boldsymbol{E}$, where χ is the dielectric susceptibility. The dielectric susceptibility is related to the permittivity through $\varepsilon = \chi + 1$. With the increasing dc-field, depending on the dielectric, the polarisation can change nonlinearly in two different ways (curves 2 and 3 in Figure 1.2). To measure the effect of a high dc-field on the complex susceptibility, a low amplitude sinusoidal voltage is superimposed onto a dc-bias $E(t) = E_{\mathrm{DC}} + E_{\mathrm{AC}} \sin(\omega t)$, where the oscillatory component E_{AC} is in the linear response region. The field dependent susceptibility is determined as $\chi = \partial P / \partial E$. The following three cases illuminate the effect of a high dc-field on the dielectric susceptibility at the fundamental frequency that are associated with both microscopic and macroscopic phenomena, whereas the apparent increase due to the electrostriction and electrode polarisation are disregarded. The interfacial polarisation is mentioned due to its relevance in cellulosic insulating materials examined in this work.

1. χ remains virtually constant despite the increased bias field. Most solid polymeric insulators exhibit such behaviour. In fact, in solid dielectrics, the local electric field acting on dipoles is largely influenced by the electrostatic interaction of dipoles. Hence, the local field causing the polarisation of a dipole, may significantly differ from the externally applied field. The fact that the susceptibility is insensitive to the increase of the external field indicates that the local field is affected insignificantly. At extremely high fields, χ can increase due to ionisation processes followed by an imminent breakdown.

2. χ increases with the bias field. The curve $P(E)$ bends upwards from the linear regime. For example, in polar liquids, the strong electric field can influence the chemical equilibrium of the sub-

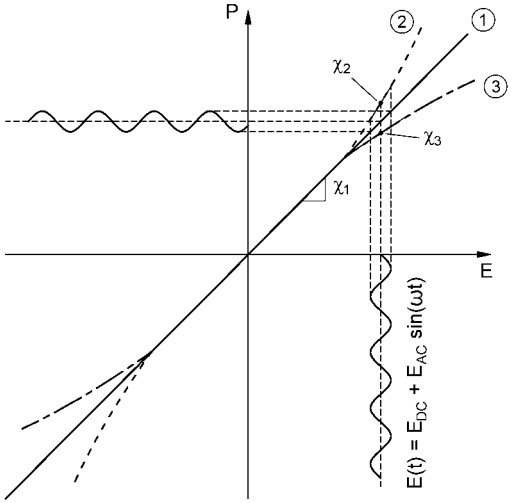

Figure 1.2: Schematic dependence of the polarisation on the electric field adapted from Figure 1 on page 102 of reference.[12]

stance. The new equilibrium has a greater dipole moment since molecules tend to align in the field direction that results in a relative increase of permittivity in the order of 10^{-6} to 10^{-3}.[13] In a solid dielectric with a rigid dipolar structure, a change of the dipole moment under a high electric stress is rather unlikely. In electrically heterogeneous dielectrics, one can expect an increase of χ due to the enhancement of the Maxwell-Wagner-Sillars polarisation as the cause of a macroscopic charge accumulation at boundaries between regions of different conductivities. Also, the hopping of ions under the influence of a static field in a disordered structure can be associated with a charge relaxation that affects the dielectric susceptibility.

3. χ decreases with the bias field. This phenomenon is known as dielectric saturation[12] or normal saturation[14] that resembles a

similar effect in magnetic materials. This effect was reported in a wide range of polar liquids,[15] and polymer solutions.[16] It is assumed that a strong electric field constrains the rotatory motions of dipoles and thereby leads to a decrease of the susceptibility. Macroscopically, the blocking of free ions within a heterogeneous dielectric can cause a substantial decrease of χ.[17–20]

1.2 High DC-Field and Dielectric Properties of Oil-Paper Insulation

The influence of high bias fields on dielectric properties of the oil-impregnated paper insulation has been drawing attention of scientists since the middle of the last century.[18,21–27] Experimental and theoretical works were motivated primarily by the need of understanding of dielectric phenomena in the insulation of power devices that can be subjected to significant bias fields, e. g. compensation capacitors or HVDC transformers. An early systematic research on the field dependence of the loss tangent of liquid impregnated dielectrics was carried out by Garton.[17] He investigated thin films of liquid dielectrics as a model approximation of pores of the paper. The author suggested, that at high alternating fields of power frequency, a fraction of ions blocked at fibre-oil boundaries cannot move with the electric field. It elucidates the reduction of the dielectric loss tangent with the increasing ac field strength. This theory was employed by later researchers in the discussion of the decrease of the loss tangent due to a high static field. Liebscher and Held[18] concluded, that of different factors determining the total dielectric loss of an oil-impregnated paper, only the loss due to the motion of ions in the liquid can decrease with the ac-field (Figure 1.3). Dipolar losses in paper and oil were assumed to be independent on the electric field in the range of magnitudes occurring

in practice. The reduction of the loss tangent due to a high dc-field was observed primarily on capacitors that had been in operation for several years, during which ionic impurities emerged in the insulating liquid.[22] The conclusion of Garton was later extended by a statement, that the increase of the loss tangent at weaker ac-fields was associated with space charge formation.[28] Depletion of charge carriers of oil under the action of a high bias field was also reported by Taschner.[27] He suggested that the accumulation of charge carriers of oil at the boundaries of cellulose fibres restricts the motion of ions in cellulose thus decreasing the loss tangent. The author mentioned that an oil film between the electrodes and the paper led to an earlier increase of the loss tangent with the bias field.

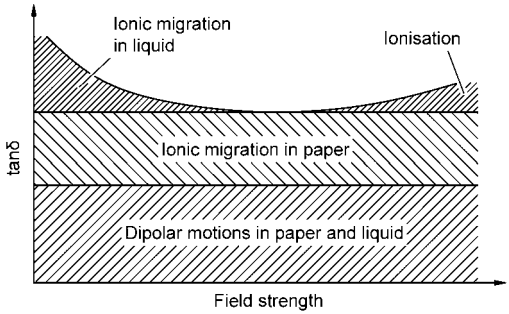

Figure 1.3: Field-dependence of loss tangent components of oil-impregnated paper at room temperature. Adapted from reference.[18]

The influence of high dc-fields on the permittivity of paper was not considered or assumed negligible in literature. On the one hand, the insensitivity of dielectric properties of a new oil-paper insulation to high dc-fields seems to be appropriate (see discussions on page 3) The ionic content of both solid and liquid phases are still low. On the other hand, it may well be anticipated that, with the progressive ageing, besides the ionic contribution of the liquid, properties of the

deteriorated paper can be influenced by the dc-field. One of the main consequences of ageing of cellulosic insulation is the increase of the water content. The hydration of cellulose significantly enhances its dielectric loss tangent and the dc-conductivity. Water can be absorbed from the ambient atmosphere or appear during the depolymerisation of cellulose chains or through ageing of oil. It seems to be reasonable to separately investigate the dielectric behaviour of cellulose, since the relaxation processes of cellulose vastly determine the amount of dielectric loss dissipated in an oil-impregnated paper. Attention to the role of water on dielectric processes in cellulose under the application of a mixed electric field should be paid.

1.3 Objectives

The intention of the present work is to characterise the dielectric relaxation processes in cellulosic insulating papers subjected to a mixed electrical stress with a high dc-component. The problem will be addressed by completing the following steps:

- Information on the low-field dielectric relaxation processes applying for cellulose will be reviewed in order to sensibly address the effects occurring in cellulosic papers under the influence of a high static field. Attention will be paid to the effects of the hydration and the polymer morphology of cellulose.
- An experimental setup and a signal processing software will be established that enable measurements of the complex permittivity under a simultaneously applied dc-field. A test cell will be assembled in which the sample preparation under vacuum as well as dielectric measurements at a controllable temperature can be carried out. A separate facility for drying and degassing of insulating oils will be prepared.
- Experiments will be carried out both on non-impregnated and oil-impregnated specimens with different water contents at different temperatures. The experimental methods will include time-resolved measurements of dielectric properties of specimens subjected to high static fields, the low-field dielectric spectroscopy and scans of dielectric spectra under simultaneously applied strong dc-fields.
- Analysis of the experimental data will be provided. Models characterising the dielectric behaviour of cellulosic paper materials will be suggested. Conclusions regarding the suitability of cellulosic papers for the use in medium-frequency transformers will be drawn.

2 Theoretical

Following discussions are based on the analysis of frequency spectra of the complex permittivity and conductivity. The present section provides therefore a brief review of the ac-response theory that includes the essential relations, relevant for the interpretation of results. Further, a method of eliminating the conductivity contribution in $\varepsilon''(\omega)$-data is presented.

2.1 AC Response Function

The time-dependent polarisation of a dielectric in a time-dependent electric field is defined in the linear regime by a response function $f(t)$

$$P(t) = \varepsilon_0 \int_0^\infty f(t)E(t-\tau)d\tau\,. \tag{2.1}$$

The response in the frequency domain is expressed by the Fourier transform of the previous equation

$$P(\omega) = \varepsilon_0 \chi(\omega)E(\omega)\,, \tag{2.2}$$

where $\chi(\omega) = \chi'(\omega) - i\chi''(\omega)$ is the complex susceptibility defined as the Fourier transform of the response function. The real and imaginary parts of the complex susceptibility are defined through

$$\chi'(\omega) = \varepsilon_0 \int_0^t f(\infty)\cos(\omega t)dt\,, \tag{2.3}$$

$$\chi''(\omega) = \varepsilon_0 \int_0^t f(\infty)\sin(\omega t)dt\,. \tag{2.4}$$

Therefore, $\chi'(\omega)$ and $\chi''(\omega)$ cannot be independent. Since they are derived from the same function $f(t)$, by using Kramers-Kronig relations, $\chi'(\omega)$ can be determined from $\chi''(\omega)$ and vice versa:

$$\chi'(\omega) = \frac{2}{\pi} \int_0^\infty \chi''(x) \frac{x}{x^2 - \omega^2}\, dx, \tag{2.5}$$

$$\chi''(\omega) = -\frac{2}{\pi} \int_0^\infty \chi'(\omega) \frac{\omega}{x^2 - \omega^2}\, dx. \tag{2.6}$$

$\chi(\omega)$ is the response function of a dielectric to a harmonic excitation at frequency ω. It can be expressed in terms of the complex permittivity

$$\varepsilon(\omega) = \varepsilon'(\omega) - i\varepsilon''(\omega) = \varepsilon_0[1 + \chi'(\omega) - i\chi''(\omega)] \tag{2.7}$$

or in terms of the complex conductivity

$$\sigma(\omega) = \sigma'(\omega) + i\sigma''(\omega) = \omega\varepsilon_0\varepsilon''(\omega) + i\omega\varepsilon_0\varepsilon'(\omega). \tag{2.8}$$

The loss tangent is determined as the relation between imaginary and real components of the complex permittivity

$$\tan\delta(\omega) = \frac{\varepsilon''(\omega)}{\varepsilon'(\omega)}. \tag{2.9}$$

The current through the dielectric is composed from the direct current and the displacement current

$$I = \sigma_{\mathrm{dc}} E + \partial D/\partial t. \tag{2.10}$$

The Fourier transform of this expression gives the response in frequency-

domain[29]

$$I(\omega) = \sigma_{dc} E(\omega) + i\omega D(\omega) t\,. \tag{2.11}$$

Considering that $D(\omega) = [\varepsilon_0(1+\chi(\omega)]E(\omega)$ and by substituting the expression for the complex permittivity (Eq. 2.7) the Equation 2.11 is modified into

$$I(\omega) = [\sigma_{dc} + \omega\varepsilon_0\varepsilon''(\omega)]E(\omega) + i\omega\varepsilon_0\varepsilon'(\omega)E(\omega)\,. \tag{2.12}$$

The first term of Equation 2.12 corresponds to the power loss due to conduction and polarisation mechanisms while the second term does not contribute to the loss. Therefore, the constant ε'' is accounted for the dielectric loss.

2.2 Separation of Conduction and Polarisation Losses

It is common to analyse the dielectric data by examining the loss peaks in dielectric loss spectra $\varepsilon''(\omega, \mathrm{T})$. However, since the dielectric loss contains the contribution of the dc-conduction

$$\varepsilon''(\omega, T) = \varepsilon''_{pol}(\omega, T) + \frac{\sigma_{dc}(T)}{\varepsilon_0 \omega}\,, \tag{2.13}$$

the information on the polarisation $\varepsilon''_{pol}(\omega, T)$ can become unreadable when the second term of Equation 2.13 becomes dominant. This can be observed in dielectrics with a high conductivity, including wet cellulose. Loss peaks due to dipolar polarisation processes can partly or completely be overshadowed, since, due to the high conductivity, the low frequency part of $\varepsilon''(\omega)$ falls off with a slope close to -1 (Figure 2.1-a). Furthermore, macroscopic polarisation effects, e g. Maxwell-Wagner-Sillars-polarisation or the electrode polarisation constitute large loss peaks at lower frequencies (Figure 2.1-b). These

dielectric features make the examination of dipolar polarisation mechanisms almost impossible. The problem can be overcome by cancelling the conductivity term in Equation 2.13.

Van Turnhout and Wübbenhorst[30] proposed a method enabling the extraction of the polarisation term of Equation 2.13 by calculating the logarithmic derivative of $\varepsilon'(\omega)$. This method is based on the fact that ε' and ε'' are related through the Kramers-Kronig equations (cf. Equations 2.5 and 2.6)

$$\varepsilon'(\omega) = \varepsilon_\infty + \frac{2}{\pi}\int_0^\infty \varepsilon''(x)\frac{x}{x^2-\omega^2}\,dx, \tag{2.14}$$

$$\varepsilon''(\omega) = \frac{\sigma_{dc}}{\varepsilon_0\omega} + \frac{2}{\pi}\int_0^\infty \varepsilon'(x)\frac{\omega}{\omega^2-x^2}\,dx. \tag{2.15}$$

As seen in Equation 2.14, ε' is determined only by the polarisation term of ε''. Hence, by calculating ε'' from ε', one can eliminate the contribution of the dc-conductivity. The expression for the polarisation loss reads

$$\varepsilon''_{pol}(\omega) = -\frac{\pi}{2}\frac{\partial\varepsilon'(\omega)}{\partial \ln\omega} \approx \varepsilon''(\omega). \tag{2.16}$$

Details of the derivation of Equation 2.16 are given in reference.[31]

Figure 2.1 illustrates how the logarithmic derivative works on model spectra with a dominating dc-conductivity (a) or MWS-polarisation (b). In case (a), the curve with empty symbols represents a typical spectrum of a conductive dielectric with a polarisation loss peak at 10 Hz. Compared to the original data, the logarithmic derivative only shows the polarisation loss. In case (b), the original spectrum features two peaks, whereas the peak due to the Maxwell-Wagner-Sillars-polarisation has a larger magnitude than the loss peak of interest. The

MWS-peak is modelled with the Debye function with the maximum at 0.1 Hz. Its shoulders are sloped by $\propto f^{-1}$ in double logarithmic axes, since $\varepsilon''_{\mathrm{MWS}}(\omega) \propto \omega\tau_{\mathrm{D}}/(1+\omega^2\tau_{\mathrm{D}}^2)$. The polarisation peak is modelled with the Cole-Cole function $\varepsilon^*_{\mathrm{CC}} = \varepsilon_\infty + \Delta\varepsilon/(1+(i\omega\tau_{\mathrm{CC}})^\beta)$ with a peak at 10 Hz. Unlike in the case (a), in case (b) both peaks remain in the spectrum of the logarithmic derivative of ε'. However, the shoulders of the MWS-peak fall off faster, i. e. $\propto f^{-2}$, separating two peaks from each other.

The described method is applicable to experimental data measured at logarithmically spaced frequencies. The derivative was calculated in MATLAB by implementing built in functions. The logarithmic derivative is sensitive to the inaccuracy and noise in $\varepsilon'(\omega)$. Therefore, the ε'-data was smoothed out with the aid of the polynomial Savitzky–Golay filter. The experimental data was extended in both directions by one point by a spline extrapolation, in order to avoid loss of data points due to the numerical differentiation.

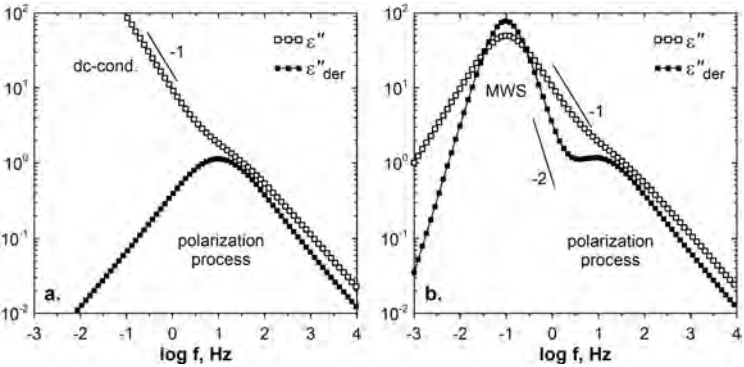

Figure 2.1: Model spectra demonstrating the extraction of a polarisation peak from the spectra dominated by a strong dc-conductivity (a) or Maxwell-Wagner-Sillars-polarisation (b) obtained with the aid of the logarithmic derivative $-\partial\varepsilon'/\partial\ln\omega$.

3 Cellulose

Insulating papers are produced from unbleached wood or cotton fibres or their mixture. The paper or pressboard are made by pressing the wet pulp without the aid of bonding agents. Figure 3.1 reveals the fibrous structure of a thermally untreated insulating paper. The micrographs show closely meshed fibres that are interlinked through thin micelles. The common method of fibre extraction in the electrical papermaking is known as the kraft process, where wood is delignified in the water solution of NaOH and Na_2S, i. e. kraft liquor. Lignin, waxes and other impurities are dissolved in the liquor solution and washed out with water. The extracted wood fibres mainly consist of natural cellulose I_β with residues of hemicelluloses, lignin and other inorganic impurities (Table 3.1). The cellulose content of cotton fibres is higher than of wood fibres and typically reaches 94 %.[32] The average degree of polymerisation, i. e. the number of monomers in one molecule of cellulose, ranges from 1100 to 1200.[33] The fibre length depends on the type of the raw material. Softwood fibres are longer and coarser than hardwood fibres, up to 6 mm in contrast to 1.5 mm. The diameter of fibres can reach 70 µm. The fibres of cellulose are hollow inside and have a braided structure made of even thinner strands (Figure 3.2). Each cellulose fibre consists of thinner macrofibrils that can be recognised on the micrograph. A macrofibril consists of even thinner microfibrils that includes up to 50 parallel chains of cellulose.

Table 3.1: The chemical composition of the wood pulp used in the electrical papermaking.[34]

75 - 85 %	Cellulose
10 - 20 %	Hemicelluloses
2 - 6 %	Lignin
< 0.5 %	Inorganics
6 - 8 %	Water

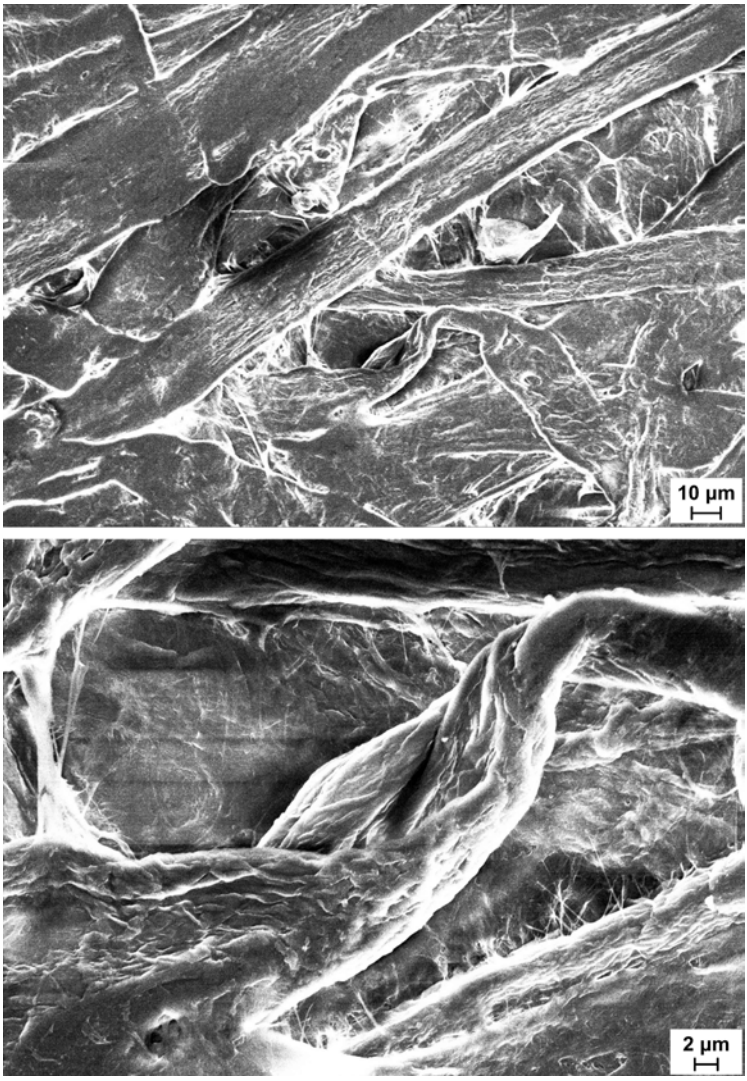

Figure 3.1: Scanning electron micrographs of an untreated insulating paper made of Kraft fibers.

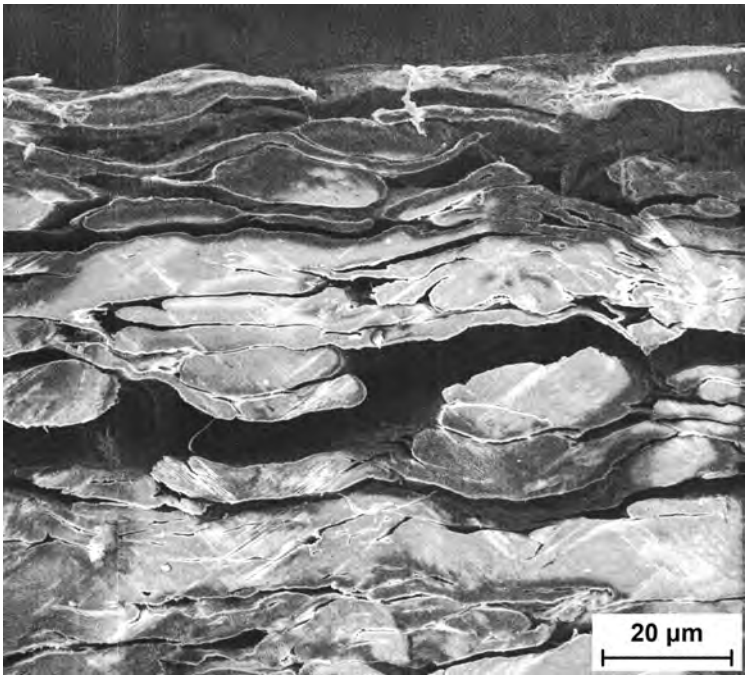

Figure 3.2: Scanning electron micrograph of the cross section of insulating paper Grade K. The sample was prepared with ion beam slope cutting with Leica EM RES102.

3.1 Structure of Cellulose

Cellulose is a natural polymer from the group of polysaccharides, composed of β-D-glucose residues that are connected through 1,4-glucosidic bonds, i. e. at carbon atoms C1 and C4 (cf. Figure 3.3). Besides glucosidic bonds, the residues are linked through intramolecular hydrogen bonds O(3)H – O5 and O(2)H – O6, running parallel to the chain direction on both sides of the main linkage. The intramolecular H-bonds stabilise the chain molecule giving it a ribbonlike shape. Neighbouring chains are linked through intermolecu-

lar hydrogen bonds between O(6)H – O3, which lie in the same plane as the intramolecular hydrogen bonds. Herewith, parallel ribbonlike chains are arranged into sheets. Groups of parallel sheets form the crystal lattice; regions with closely packed sheets are called crystallites. Crystallites of cellulose and chitin exhibit a particularly tight packing compared to other polysaccharides that explains their insolubility in water in spite of the exceptional ratio of hydroxyl groups per monomer.[35] Groups of disordered molecules are considered as amorphous regions (Figure 3.4). The degree of crystallinity in the natural cellulose depends on the mechanical, chemical and thermal pretreatment and varies from 20 to 90 %.[36] The average degree of crystallinity of cellulose in the insulating kraft paper measured 80 % according to the X-ray diffraction analysis.

3.2 Cellulose and Water Interaction

Like other polysaccharides, cellulose has a significant hydrophilicity, since each of the three hydroxyl groups of each monomer can bind a molecule of water through hydrogen bonding. The adsorption of water onto the macromolecule of cellulose is uneven due to the unsymmetrical conformation of the polymer. The OH-group at the branch C_5-C_6 stands out further than two other OH groups at C_2 and C_3 (Figure 3.3). The longer OH group has a higher chemical activity that also applies for the binding of the water molecule. As mentioned earlier, the degree of crystallinity, i. e. the fraction of amorphous regions, determines the degree of hydration of cellulose. Under room conditions the insulating paper made of wood of cotton fibres adsorbs in average up to 8 % wt. moisture, while wood fibres contain slightly more moisture than cotton fibres.

The hydrophilicity of cellulose is an important morphological feature that manifests itself in dielectric, mechanical and other phys-

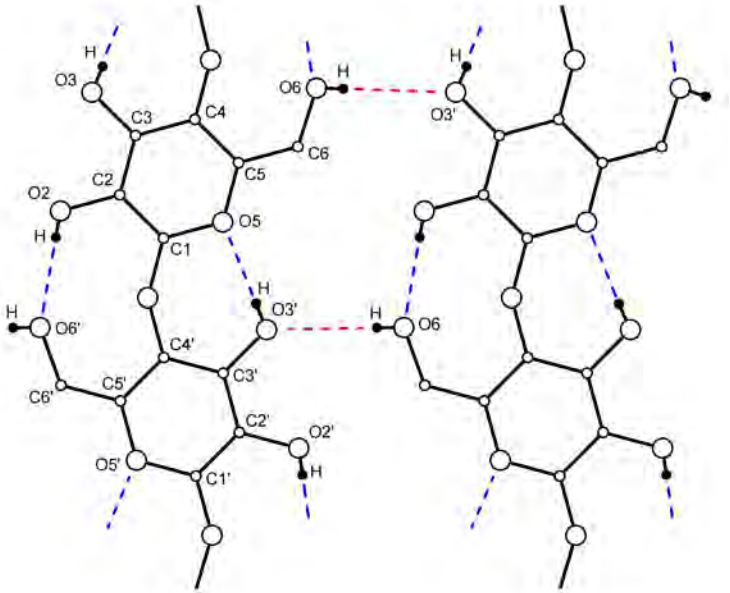

Figure 3.3: Molecular arrangement of natural cellulose in a crystalline region with intramolecular (blue) and intermolecular hydrogen bonds (red).

ical properties. Lindh et. al.[37] suggest that the outer surfaces of microfibrils are composed of cellulose chains with a more disordered side group arrangement that are easily attracted to water molecules (Figure 3.4). In contrast, the chains at inner surfaces of microfibrils exhibit a lower accessibility to water.

It is known that the physical properties of water adsorbed in cellulose are different from those of bulk water. At lower degrees of hydration water molecules are directly attached to cellulose macromolecules. At higher degrees of hydration secondary layers of water molecules are formed. These molecules of water do not directly interact with hydroxyl groups of cellulose and exhibit properties close to

those of bulk water. Based on differential scanning calorimetry (DSC), three forms of water adsorption in cellulose are distinguished.[38]

- *Nonfreezing bound water* – water molecules closely attached to cellulose macromolecules through hydrogen bonds. This type of adsorbed water does not turn into ice below the freezing temperature because of the distance between single water molecules.
- *Freezing bound water* – water molecules directly attached to cellulose connect further water molecules via hydrogen bonds. In this case, the occurrence of ice crystals can be detected in a DSC-measurement.
- *Free water* – at higher levels of hydration, amorphous clusters of water are formed. When cooled down, such clusters turn to ice crystals similar to pure water. The main difference between free and freezing bound water is that bound water molecules are more restricted in motion through hydroxyl groups of cellulose.

Water has a detrimental influence on the electrical and mechanical properties and the thermal stability of the cellulosic insulation.

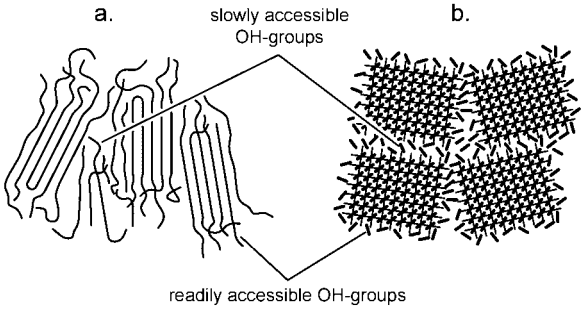

Figure 3.4: Schematic structure of a macrofibril with lines representing chain molecules of cellulose (a). The cross section of a bundle of four microfibrils (b).

The adsorption of water accelerates the thermal ageing of cellulose that leads to shortening of chain molecules through depolymerisation. Only under the maintenance of a high degree of dryness of the oil-paper insulation can a long-term reliability of the transformer be ensured. The maximum permissible degree of hydration of the transformer insulation is between 0.3 and 1 % wt.[39] The higher the voltage rate of the transformer, the higher the requirement for the dryness of the insulation.

In the course of the operation, water is adsorbed from the atmosphere through parts of the insulation exposed to the moist air. It is also produced through the chemical depolymerisation of cellulose and decomposition of oil under the influence of high thermal and electrical stresses. The moisture distribution between oil and paper depends on the temperature of the insulation and ambient temperature and humidity. The cellulosic paper takes in the most part of water due to its greater hydrophilicity. While the mass fraction of water in cellulose is measured in per-cents by weight, the moisture content of oil is typically measured in parts per million. The solubility of water in oil increases with the temperature. A more detailed account on the effect of water on dielectric properties of cellulose will be given in a separate section.

4 Dielectric Relaxations in Cellulose

The following section describes the dielectric relaxation processes in cellulose including ionic and dipolar mechanisms that define the values of ε' and ε'' in the frequency range from several mHz up to several MHz. Prior to the introduction of dipolar relaxation mechanisms in cellulose, a brief account of dielectric relaxations in polymers in the glassy amorphous state is given. Therewith, molecular motions defining the origins of dipolar relaxations in a wide range of polymers are illuminated.

4.1 Ionic Transport

The dielectric response of cellulose to an external electric field is determined by the polarisation of permanent dipoles and the motion of free ions. The mechanism of ionic transport in cellulose is similar to that of ionically conducting amorphous solids, e. g. glasses. In what follows a brief discussion of the ionic conduction and the associated dielectric relaxation is provided.

The conductivity of cellulose is determined by the transport of ions that hop between neighbouring stable sites by surmounting potential energy barriers when acquiring sufficient thermal energy. Cellulose may contain protons that occur in an ion exchange reaction when the pulping chemicals are washed out with distilled water. It can also contain alkali metal ions remaining after the washing. The proton transport involves two different mechanisms. The first mechanism implies a transition of a proton between covalent OH and hydrogen bonds (Figure 4.1-a). A bare proton appearing at the left end of the chain, forms a positive OH_2^+ ion that is transported to the right end by a sequential hopping of a successive proton. After passing of the proton, the chain is again in the confirmation (b) that does not permit a transit

of a new proton in the same way. In this case, the second mechanism applies, where the proton is transferred through rotations of hydroxyl groups. After passing of the proton the configuration of OH-groups returns to the form shown in Figure 4.1-a. The conductivity of cellulose is sensitive to hydration, since water molecules together with the OH-groups of cellulose build conduction paths, along which protons and alkali ions can move around.[40,41] Murphy[40] suggested a power-law dependence of the conductivity on the water content, expressed through $\sigma = \sigma_s(\alpha/\alpha_0)^n$ with $n = 9$, where σ_s is the saturation conductivity and α/α_0 is the relative water content.

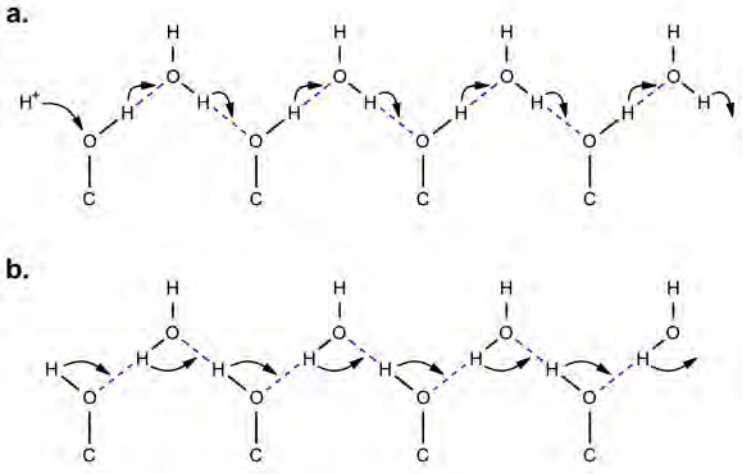

Figure 4.1: Transport of an proton entering the chain on the left side through the exchange of the covalent OH- and hydrogen bonds (a). Proton transport through the rotation of OH-bonds (b). Adapted from Nagle.[42]

The disordered structure of cellulose implies a random distribution of potential energies of varying heights and depths. In hydrated amorphous regions featuring water bridges between cellulose chains

and water phases, the potential barriers can be lower than in crystalline regions. In presence of water, an ion has more options for a further move. In crystalline regions, hydroxyl groups are engaged in intra- and intermolecular hydrogen bonds that prevents an ionic transport (cf. Figure 3.3). The probability of hopping over a barrier of height ΔH is defined as $\exp(-\Delta H/k_B T)$, where k_B is Boltzmann's constant and T is the temperature. Under an external electric field the distribution of potential barriers tilts as shown in Figure 4.2. The probability of transition in the field direction increases to

$$k = \exp(-(\Delta H - qEd/2)/k_B T)\,, \tag{4.1}$$

where q is the ion charge, d is the distance between the adjacent sites. The probability of a jump in the opposite direction decreases according to

$$k' = \exp(-(\Delta H + qEd/2)/k_B T)\,. \tag{4.2}$$

The number of sites to which an ion can hop is restricted due to different barrier heights and since not all surrounding sites can be vacant. On a short time scale, an ion jumps over smaller barriers in a zig-zag trajectory exploring shorter distances. On a longer time scale, higher barriers that define the dc-conduction can be surmounted that results in ionic transport over longer distances.

Not all ions can participate in the conduction process at the same time, since some of them can be trapped in deep sites. With increasing temperature, thermally activated ions leave the traps with greater ease thus increasing the conductivity. The temperature dependence of the conductivity follows the Arrhenius relation

$$\sigma_{\mathrm{DC}} = \sigma_\infty \exp(-\Delta H_{\mathrm{DC}}/RT)\,, \tag{4.3}$$

where σ_∞ is the pre exponential factor, ΔH_{DC} is the activation energy,

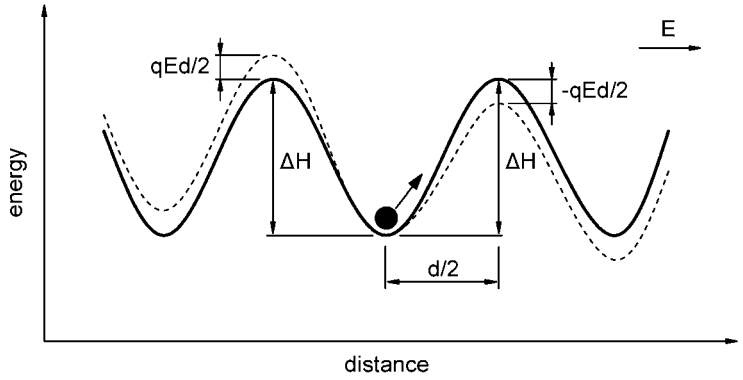

Figure 4.2: Deformation of potential barriers upon the application of an electric field E.

$R = 8.314$ J/(mol · K) is the gas constant.

Taylor[43] noted that the activation energy of the dc-conduction and a dielectric relaxation observed at low frequencies is nearly equal in a wide variety of glasses. It was interpreted that both conduction and low frequency relaxation processes originate from the motion of the same ionic species. Later, a relation between the dc-conductivity and the parameters of the dielectric relaxation was suggested[44,45]

$$\sigma_{\mathrm{DC}} = p\varepsilon_0 \Delta\varepsilon 2\pi f_m \,, \tag{4.4}$$

where p is a correlation factor, ε_0 - permittivity of vacuum, $\Delta\varepsilon$ - relaxation strength of the dielectric loss peak with the peak frequency f_m. In fact, the spectral shape of $\sigma'(\omega)$ is universal for a wide range of materials (Figure 4.3-a).[46] The point at which the conductivity bends from the plateau of the dc-conductivity is called critical frequency ω_c. The critical frequency corresponds to a peak in the dielectric loss spectrum. The relation $\sigma_{\mathrm{DC}} \sim \omega_c$ holding for the critical frequency is known as Barton-Nakajima-Namikawa relation. Above ω_c the ac-conductivity

obeys a universal relationship[46]

$$\sigma'(\omega) - \sigma_{DC} \propto \omega^{s(\omega,T)}, \tag{4.5}$$

with $s(\omega,T) \in [0.6;1]$.

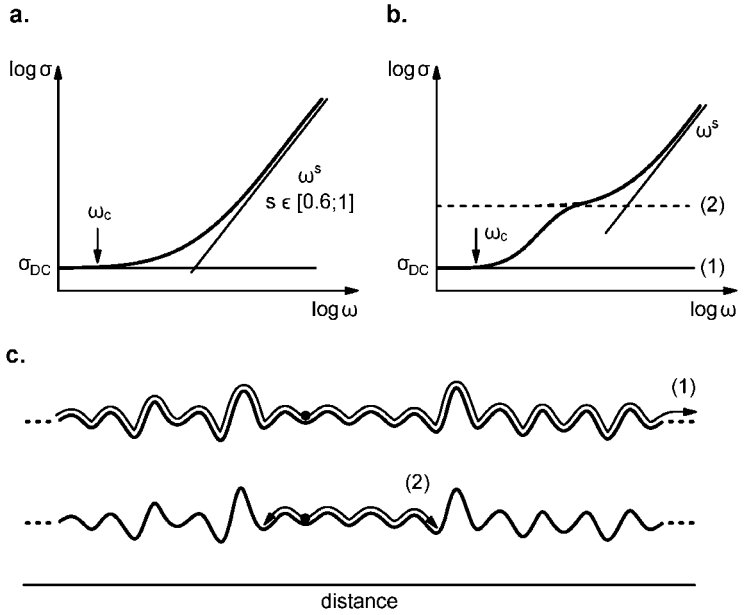

Figure 4.3: Schematic of the universal shape of the frequency spectrum of the real part of the complex conductivity (a), the effect of a localised diffusion process on the frequency spectrum of σ' (b), schematic of a one dimensional potential barrier with non-localised (1) and localised (2) diffusion processes (c).

In some electrically heterogeneous materials, a knee-like feature as schematically shown in Figure 4.3-b can be observed in the conductivity spectrum.[47,48] Namikawa[45] reported that glasses generally feature at least two different diffusion processes – non-localised and localised (Figure 4.3-c). A non-localised diffusion process is related

to the dc-conduction in terms of equal activation energies. It is marked by a large loss peak. In contrast, a localised diffusion process does not affect the dc-conduction. It is associated with a loss peak in $\varepsilon''(\omega)$ arising at a higher frequency and a knee-like bend in $\sigma'(\omega)$ that is attributed to the Maxwell-Wagner-Sillars relaxation.[49]

The electrical heterogeneity of the cellulosic paper that is related to the fibrous structure and to the semicrystalline morphology of cellulose implies the presence of domains of low and high conductivity, e. g. the crystalline and amorphous regions (Figure 4.4). As mentioned earlier, the conductivity of amorphous regions increases due to the adsorption of water. It is commonly assumed that the motion of ions in conductive amorphous regions is blocked by less conductive crystallites or at larger-scale interfaces. Piles of positive and negative charges arise at opposite sides of less conductive zones. Such separation of charge behaves in an alternating electric field like a dipole of a large dipole moment. Especially at lower frequencies, the separation of charge increases the permittivity. This phenomenon is typical for electrically heterogeneous materials with a highly conductive component as the Maxwell-Wagner-Sillars-relaxation.

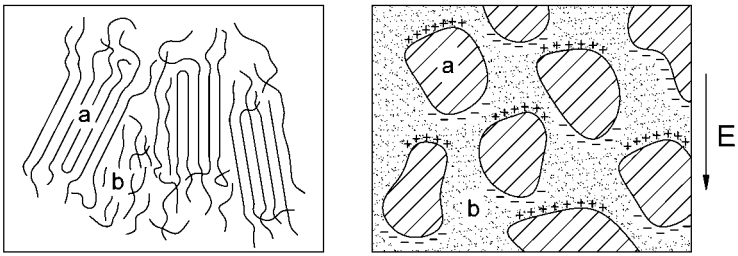

Figure 4.4: Schematic of the Maxwell-Wagner-Sillars-relaxation in a semicrystalline material with non-conductive crystallites (a) and conductive amorphous regions (b).

4.2 Relaxations in Polymers in the Glassy State

There are different states, in which a polymer may exist: amorphous or semicrystalline (glassy), viscoelastic fluid (rubber) and viscous fluid. The glass-rubber transition in amorphous polymers appearing at the temperature T_g causes major structural changes accompanied by significant alterations of mechanical, dielectric, thermal and other physical properties. This transition is designated as the primary or α-relaxation. Semicrystalline polymers exhibit further structural transitions due to crystalline phases. The latter are treated in detail in literature.[50]

It is customary to denote the relaxation mechanisms in polymers with Greek letters α, β, γ, etc. according to the temperature, at which these relaxations set in ($T_\alpha > T_\beta > T_\gamma > T_\delta$) when measured isochronally ($\omega = \text{const}$), or according to frequencies of loss peaks ($\omega_\alpha < \omega_\beta < \omega_\gamma < \omega_\delta$) when measured isothermally ($T = \text{const}$).

In the glassy state, amorphous polymers or amorphous phases of semicrystalline polymers possess at least one, mostly two secondary relaxations β and γ. In contrast to the primary relaxation, secondary relaxations originate from lower range molecular motions featuring broader and lower loss peaks than the α-peak.

The temperature dependence of the β-relaxation obeys the Arrhenius law

$$\omega_p(T) = \nu_0 \exp\left(\frac{E}{kT}\right), \tag{4.6}$$

where $\omega_p(T)$ is the frequency of the loss peak, ν_0 is the relaxation rate in the high-temperature limit, E is the energy of activation.

Figure 4.5 depicts the β-peak of poly(methyl methacrylate) (PMMA) due to the motion of the ester group around the C–C bond connecting the side group to the main chain. With increasing temperature, the sterical hindrance for the side group rotation ceases and the

β-peak shifts towards higher frequencies at a growing peak magnitude.

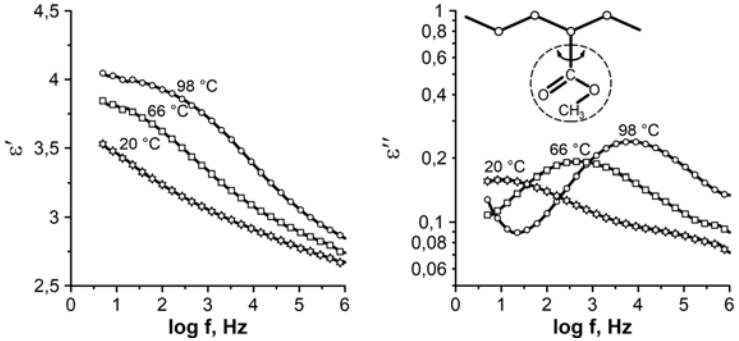

Figure 4.5: β-relaxation in poly(methyl methacrylate) (PMMA). Measurements were carried out by the author using techniques described in Section 5.

4.3 Molecular Origin of Secondary Relaxations

Understanding the molecular origin of the secondary relaxations has an important practical value. In polymeric insulators, dielectric losses at typical operating frequencies and temperatures are mainly associated with secondary relaxation mechanisms in the glassy state. Even more so at frequencies in the range of several kilohertz, since secondary loss peaks at operating temperatures are typically located at frequencies higher than 10 kHz. A classification of molecular motions underlying the secondary relaxations has been given by Heijboer[51] based on the analysis of mechanical loss peaks in different polymers. Kolařik and coworkers[52] discussed the alterations of existing relaxations or rise of new ones due to the interaction of polymers with different low-molecular weight diluents, e. g. water, also based on

mechanical relaxation studies. Figure 4.6 combines the mechanisms described in both sources.

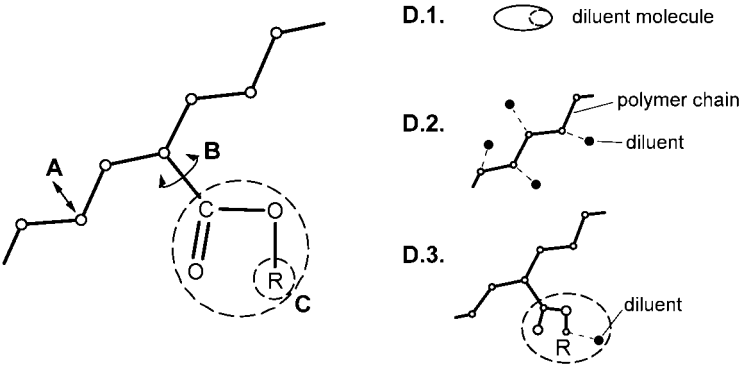

Figure 4.6: Molecular movements underlying the secondary loss peaks (illustrated after Heijboer[51] and Kolařik[52]).

- **Type A.** Local motions of short chain segments with much lower magnitude as in the α-relaxation. Example is the β-relaxation in polyvinyl-chloride (PVC) without side groups.
- **Type B.** Rotation of polar side groups around bond axes linking them to the main chain. A typical example is the β-relaxation in poly(methyl methacrylate) (PMMA) due to the rotation of the whole $COOCH_3$ group around the C–C bond (Figure 4.5).
- **Type C.** Motions within side groups, without interacting with the main chain, e. g. internal rotations within CH_3 of PMMA.
- **Type D.** Introduction of low-molecular weight diluents, such as water, into a polymer can cause different types of relaxations. In the present work, the classification provided by Kolařik and coworkers has been adopted:[52]

  D.1. *Motions of diluent molecules incorporated in a polymer.* The dynamics of diluent molecules within a polymer depends on their concentration. At lower concentrations, diluent

molecules are tightly bound to the polymer. Their mobility is significantly lower compared to the bulk liquid state; the corresponding relaxation peak denoted β_d appears at lower frequencies. With increasing concentration, weaker bound networks of diluent molecules build up. The relaxation peak grows due to the contribution of diluent molecules and shifts towards higher frequencies. Studies on water dissolved in amorphous polymers have revealed a similarity to the dynamics of water within confining environments.[53]

D.2. *Motions of diluent molecules with local motions of the main chain.* This type of interaction is characteristic for polymers without polar side chains (e. g. polyamides, poly(ethylene therepthalate)). The local motions of polar segments of the polymer backbone cease with the addition of diluents. At the same time a relaxation peak due to the motions of diluent molecules appears.

D.3. *Motions of diluent molecules with rotations inside the side groups.* Upon adding diluents, the loss peak originating from side chain motions is transformed into a loss peak due to the motions of diluent molecules.[54]

4.4 Secondary Relaxation Processes in Cellulose

As mentioned earlier, cellulose has a semi-crystalline structure of microfibrils with tightly packed crystallites and disordered amorphous phases. Like in synthetic polymers, the semi-crystalline morphology plays an important role in molecular relaxations of cellulose. In fact, the secondary relaxations discussed below are assumed to take place only in amorphous regions, where the dipoles possess a greater freedom of motion. Similarly, dielectric processes associated with the

hydration of cellulose are located in amorphous regions too. Below, a brief review of dielectric relaxation processes in cellulose is given.

The molecular interpretation of secondary relaxations in polysaccharides, including cellulose, has been controversial among different authors.[55–58] In this work definitions suggested by Kaminski and his coworkers[59] are adopted. The authors identified similarities between β- and γ-relaxations of cellulose with relaxations in mono- and disaccharides made of similar monomers as cellulose. In fact, activation energies of rotatory motions determined for example in trehalose $\Delta H_\beta = 87 \pm 1$ kJ/mol, $\Delta H_\gamma = 51 \pm 0.5$ are close to values obtained for cellulose $\Delta H_\beta = 85\pm$ kJ/mol, $\Delta H_\gamma = 38...43.5$. This assumption seems plausible due to the fact that the secondary relaxations of cellulose originate from local chain motions involving few monomers.

4.4.1 The β-relaxation

The β-relaxation is related to local rotations of several monomers around the longitudinal axis of the cellulose chain (Figure 4.7-a). Such type of polymer chain motions is known in literature as the Johari-Goldstein (JG) relaxation.[60] This form of dielectric relaxation is observed in numerous polymers in glassy amorphous state and other glass-forming materials. Local rotations within a chain molecule of cellulose with rigidly attached side groups and hydrogen bonds to the neighbouring chains, require a higher activation energy than the motion of side groups. As discussed earlier, this type of secondary relaxation can be eased through adding diluent molecules that act as a plasticiser. In dielectric loss spectra of cellulose, the β-relaxation process can be identified as a broad peak of low magnitude (see Figure 4.8-a). In a wet cellulose it is masked under the β_{wet}-peak (Figure 4.8-b).

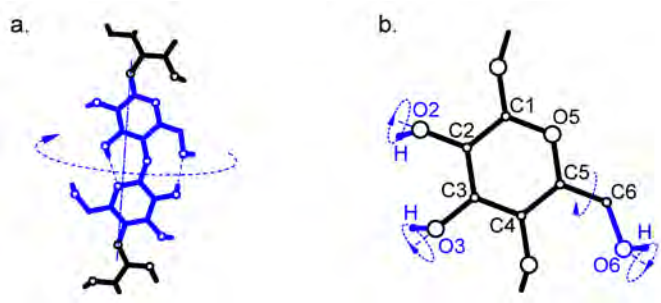

Figure 4.7: Schemes of molecular motions related to secondary relaxations in cellulose: (a) β-relaxation due to the rotation of short chain segments in conformity with the Johari-Goldstein relaxation; (b) γ-relaxation due to rotations of OH and CH_2OH side groups.

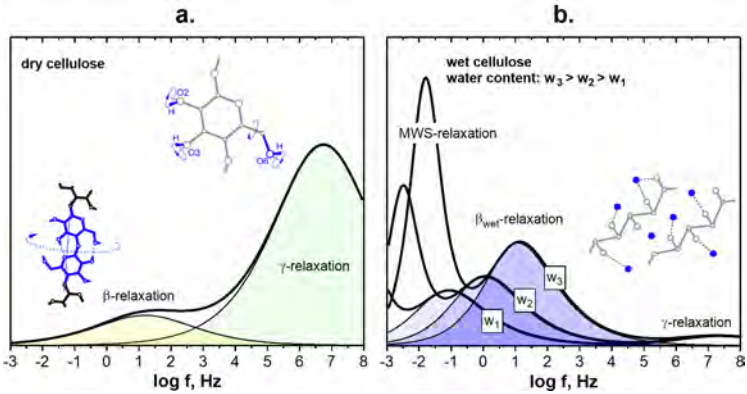

Figure 4.8: β and γ relaxations in dry cellulose as defined by Kaminski et. al.[59,61] (a). Influence of the increasing water content on dielectric loss spectrum of cellulose with omitted conductivity contribution as described in works of Einfeldt et. al.[55] (b).

4.4.2 The γ-relaxation

Cellulose has polar side groups that can rotate around their bond axes that connect them to the glucose ring unless they are rigidly

bonded with side groups of neighbouring chains as in the crystalline lattice. Their motion can be detected as a dipolar loss peak in $\varepsilon''(\omega)$ at higher frequencies. Kaminski and coworkers defined these molecular motions as the origin of the γ-relaxation in various polysaccharides, since a similar dielectric relaxation was observed in mono- and disaccharides that have the same side groups (Figure 4.7-b). This process is characterised by a lower activation energy than the β-relaxation. The hydration increases the activation energy of the γ-process, indicating that the dipolar moment of OH-groups increases through the attachment of water molecules.[55] The peak of the γ-relaxation in the dielectric loss spectrum appears at a higher frequency than that of the β-relaxation because of the shorter relaxation times of side group rotations than the rotation of bulky chain segments. The γ-process is characterised by a higher and sharper peak than the β-peak. It is also visible in the dielectric loss spectrum of wet cellulose (Figures 4.8 and 4.9).

4.4.3 The β_{wet}-relaxation

Water incorporated in cellulose, even at lower concentrations, has a significant influence on the complex permittivity of the host polymer. A specific dielectric feature for cellulose and other polysaccharides and their derivatives, that arises as a cause of hydration, is called β_{wet}-relaxation. It is marked by a pronounced loss peak that arises between 0 and 60°C on the right shoulder of the MWS-peak (Figure 4.9). The latter is also enhanced due to the hydration. The peak of β_{wet}-process vanishes almost completely upon drying and reappears again with adsorption of water. Drying the paper under vacuum removes the vast part of the water residing in amorphous regions. Dielectrically, it is associated with a permittivity decrease explained by the disappearance of the β_{wet}-peak as well as the decrease of the MWS-relaxation

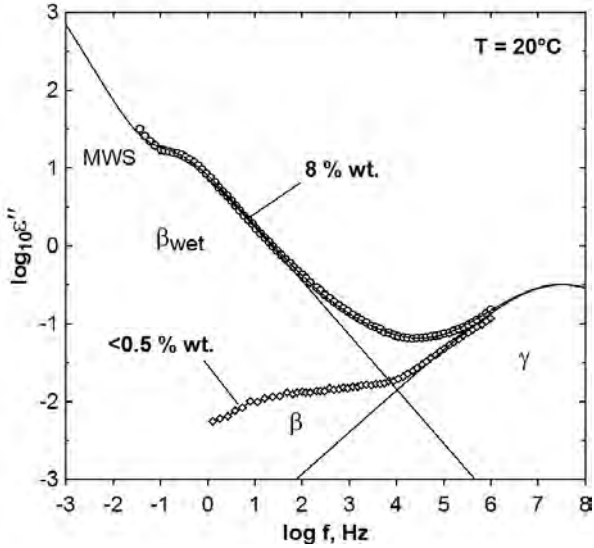

Figure 4.9: Comparison of relaxation mechanisms of dry and room-humid cellulose paper at room temperature fitted with Havriliak-Negami functions. Measurements were carried out by the author using techniques described in Section 5.

and its shift to lower frequencies (Figure 4.9). Upon drying, a very flat peak of the β-relaxation becomes visible.

The molecular origin of the β_{wet}-relaxation is a subject of uncertainty. It has been related to the proton hopping which concentration and range of motions is enhanced through the increasing water content.[56] There is an ambiguity, whether the β_{wet}-relaxation is related to the motion of polymer chains, or rather represents orientational polarisation of a gel-like structure of cellulose side groups dissolved in water.[55] Khan and Pilpel[62] suggested that water molecules, by creating bridges between hydroxyl groups of neighbouring molecules, facilitate correlated orientational motions that cause greater charge displacements. The activation energy of the β_{wet}-relaxation, as reported

in literature, measures between 63 and 70 kJ/mol.[63]

In order to characterise the β_{wet}-relaxation in an insulating kraft paper, permittivity spectra from 1 Hz to 1 kHz were measured on a room-humid specimen in a temperature range 20 to 180°C (Figure 4.10). The original spectra of $\varepsilon''(\omega)$ indicate that the dielectric loss first increases with the temperature reaching a maximum at 80°C then decreases to a minimum at 150°C followed by a new peak at higher temperatures. The shape of the loss spectrum $\varepsilon''(\omega)$ does not allow a detailed analysis of the β_{wet}-process due to the MWS-relaxation (Figure 4.10-a). In the spectrum of the logarithmic derivative of $\varepsilon'(\omega)$, the β_{wet}-peak can be observed as a saddle-like feature 1 (Figure 4.10-b). On the low frequency side of the β_{wet}-peak a larger loss peak 2 can be seen, which is ascribed to the MWS-relaxation. At temperatures above 150°C, the emergence of high-temperature relaxation peak 3 is visible.

With the increasing temperature, instead of starting to immediately decrease in magnitude, the β_{wet}-peak first shifted back to lower frequencies. In literature, the shift of the peak in the opposite direction was interpreted as the effect of drying.[63] In this source, the activation energy of the β_{wet}-relaxation was determined from the slope of the linear part of the function of relaxation time on the inverse of temperature (Figure 4.11). In the given example, the activation energy determined in this manner counted 66 kJ/mol, which is in a good agreement with results of other authors.

Interestingly, a similar behaviour of a relaxation peak was observed in hydrated porous glasses by Ryabov and coworkers.[64] The authors attributed the dielectric relaxation to the motion of water molecules in an ice-like state, i. e. molecules with a restricted range of motions. They assumed, that the probability of orientations of water molecules first increases with the temperature, but starts to decrease, when thermal oscillations become dominant at higher temperatures.

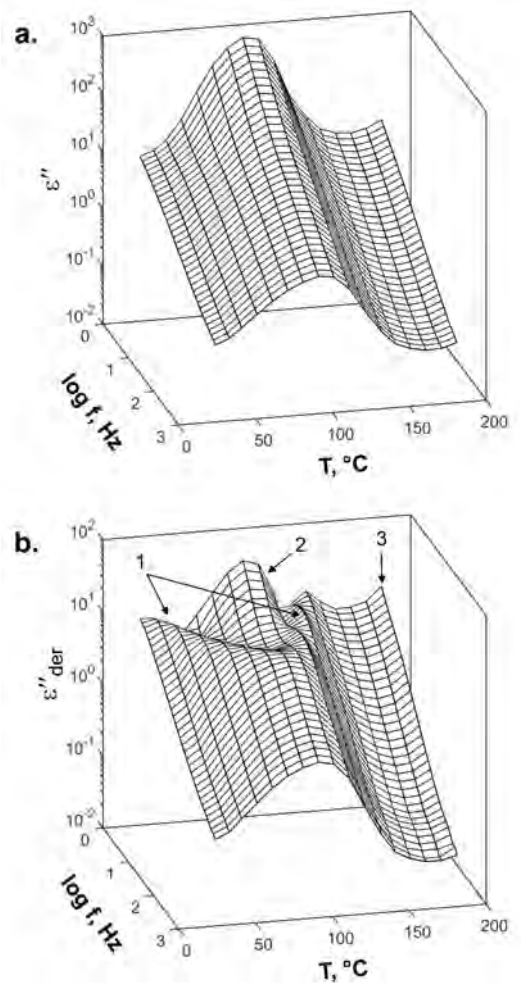

Figure 4.10: Three-dimensional plot of temperature and frequency dependent dielectric loss (a) and the logarithmic derivative of ε' (b), measured on a room-humid cellulosic insulating paper with 7 % wt. water. Measurements were carried out by the author using techniques described in Section 5.

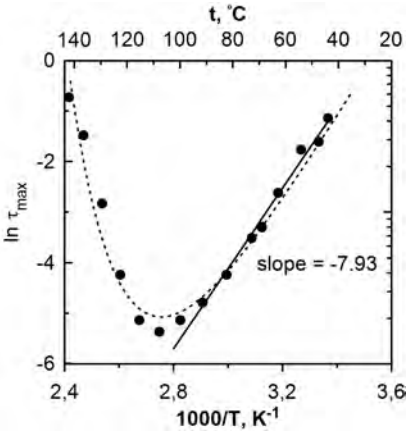

Figure 4.11: Temperature dependence of the relaxation time of the β_{wet}-process in a room-humid cellulosic insulating paper from Figure 4.10.

Another explanation for the bow-like transition of the β_{wet}-process at a maintained peak magnitude might be the migration of protons. It seems reasonable that the probability of proton motions first increases with the temperature elevation. It shifts the relaxation peaks of β_{wet}- and MWS-processes to higher frequencies. The reversal of the shift direction might be related to the increase of chaotic thermal motions, lowering the hopping probability of protons (Equation 4.1). At further heating, the concentration of water in cellulose decreases. Hence, conduction paths formed by water gradually disappear, restricting the probability of ionic hopping. The decreased conductivity of the amorphous regions also reduces the MWS-peak 2 and causes its shift to lower frequencies.

It can be assumed, that the water in the paper specimen has been removed almost completely by the moment of reaching 150°C. However, at a continued heating, the dielectric loss starts to increase again,

marking the onset of a high-temperature relaxation[47] (feature 3 in Figure 4.10-b).

4.5 Temperature Dependence of Relaxation Processes

Previously introduced relaxation processes in cellulose depend on temperature. As shown in the previous example, the increase of temperature significantly alters the dielectric properties of the hydrated cellulose due to the activation and the consequent removal of water. Practically, it can be stated, that the detrimental effect of water is enhanced by the increase of temperature within a range, where the water still remains in cellulose. Dipolar processes of dry cellulose are also affected by the change of temperature. The relaxation times of molecular motions, responsible for β- and γ-processes decrease with the temperature elevation, i. e. their peaks shift to higher temperatures.

Figure 4.12 shows frequency spectra of the complex permittivity of a dry Transformerboard specimen with less than 0.5 % wt. water. It indicates that the permittivity increases with temperature at frequencies below 1 kHz. In contrast, above 1 kHz the dielectric loss decreased with temperature. This is explained by different dynamics of corresponding relaxation processes, i. e. their different shift rates with temperature.

At lower frequencies, the increase of temperature enhances the MWS-relaxation and causes another process on the right shoulder of the MWS-peak. In literature this phenomenon is denoted σ-relaxation.[47] Such high-temperature relaxation was observed not only in various polysaccharides and their derivatives but also in conductive glasses.[65] Einfeldt and coworkers suggested that a local diffusion process, different from the MWS-relaxation, causes the appearance of a dielectric loss peak at higher temperatures, in which the motion of ions

is involved. The commensurate increase of the dc-conductivity of cellulose at high temperatures was also supported with this hypothesis.

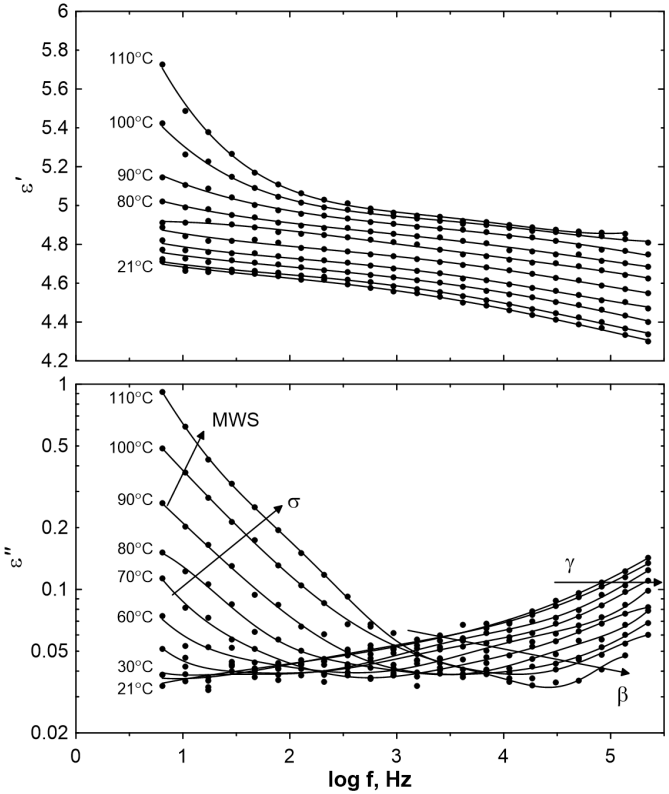

Figure 4.12: Dielectric spectra of a dried Transformerboard (< 0.5 % wt. water) measured at different temperatures. Measurements were carried out by the author using techniques described in Section 5.

Another effect of temperature on the dielectric behaviour of cellulose is possible due to alterations in the morphology of cellulose. The high temperature causes the annealing of cellulose and other organic constituents of paper. Cellulose chains break apart; the de-

gree of crystallinity of cellulose decreases. A so-called hornification takes place.[66,67] With water escaping the cellulose, chain molecules in amorphous regions are packed closer to each other. In a closer proximity of neighbouring molecules, a reestablishment of hydrogen bonds and other chemical linkings, earlier diminished through the adsorption of water, is assumed. The hornification is a partially reversible process. Therefore, a paper once subjected to high temperatures adsorbs less moisture than a thermally untreated paper.

5 Experimental

The general idea behind the experiments was to assess the alterations of the complex permittivity of insulating paper materials due to subjection to a high bias field. An experimental setup was developed by the author for the purpose of measuring the complex permittivity at a simultaneously acting high dc-voltage. In order to characterise the behaviour of the dielectric subjected to a high bias field, the intensity of the bias field and the stress duration, as well as the magnitude and frequency of the probing ac-voltage were varied. These experiments were carried out at different temperatures and water contents of specimens. The following chapter provides detailed explanations of the measurement methods, the design and function of the experimental setup and the procedure of specimen preparation.

Schemes of electric field configurations employed by the author in the present work are illustrated in Figure 5.1.

1. *Time-resolved measurement.* With a time-resolved measurement of the complex permittivity it was intended to observe the dielectric behaviour of the specimen over an extended time span after applying a high bias field. Depending on temperature and water content, ε' and $\tan\delta$ of insulating papers behaved differently. It is known that the polarisation of the dielectric upon a step voltage application evolves according to time constants of individual polarisation processes. By superimposing a low-amplitude ac-voltage of a fixed frequency, the influence of a bias field on a particular polarisation process, which is addressed with the ac-voltage, can be observed. Hence, faster dipolar processes were examined with a high frequency probing voltage, whereas slower ionic processes with a low frequency ac-voltage.
2. *Variation of mixed field components.* Preliminary measurements identified a dependence of the permittivity of paper specimens

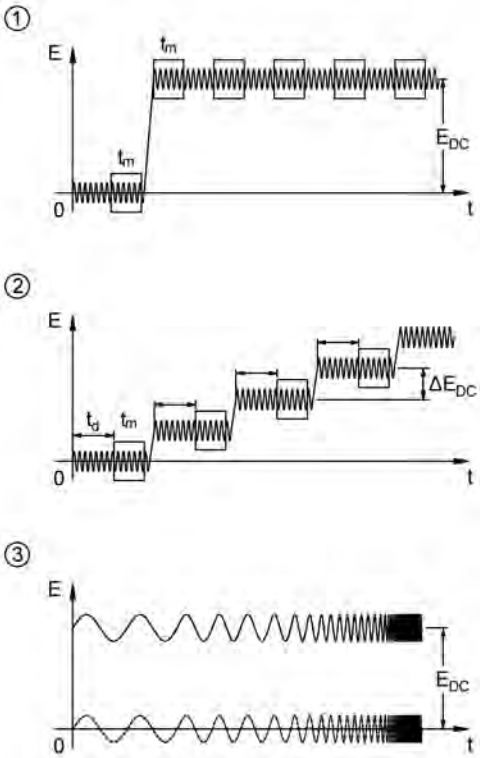

Figure 5.1: Schematic illustration of electric field configurations employed in permittivity measurements: (1) time-resolved measurement of the permittivity under the action of a bias field, (2) measurement of permittivity as a function of the bias field and probing ac-voltage, (3) dielectric spectroscopy at a simultaneously applied bias field. t_m is the width of measured signal windows, t_d is the time delay before signal measurements.

on the intensity of both ac- and dc-components of the mixed electric field. To obtain functions $\varepsilon'(E_{\mathrm{DC}})$ and $\varepsilon''(E_{\mathrm{DC}})$, the bias field was elevated in steps, whereas the complex permittivity was probed by an ac-voltage of a fixed frequency. Measure-

ments were carried out also with a high amplitude ac-voltage. Upon each step-like adjustment of the bias field, the permittivity was measured after a constant time delay t_d.

3. *Dielectric spectroscopy using a biased ac-signal.* Since the alterations of ε' and ε'' due to the bias field depended on the frequency and amplitude of the probing voltage, it was decided to examine the dielectric spectra in a wide range of frequencies under the action of a bias field. The complex permittivity and conductivity spectra were measured in a frequency range 5 Hz to 1 MHz with a low-amplitude ac-signal, and in a range 40 Hz to 500 Hz with a high-amplitude ac-signal. Measurement of one sweep from 5 Hz to 1 MHz took less than one minute. Keeping the sweep times as short as possible was important to measure instantaneous shapes of frequency spectra, considering time dependent changes of ε' and ε'' observed under dc-field. In order to minimise perturbations caused by low-frequency voltage, frequency sweeps were taken from high to low frequencies.

The equipment used in permittivity measurements included a commercial LCR-meter Newtons4th PSM 1735 with an external current amplifier FEMTO DLPCA-200 for low-voltage measurements and a home-made setup for high-voltage measurements.

5.1 Test Setup for Dielectric Measurements

5.1.1 Basics

A home-made setup for measuring the complex permittivity was based on a commercial digital oscilloscope. It consisted of two voltage dividers connected in parallel (Figure 5.2). The left part, called reference branch, contains a gas-filled high-voltage condenser of 100 pF

represented by an impedance $\underline{Z}_r$. The low-voltage part of the reference branch $\underline{Z}_{LV1}$ is a parallel connection of input elements of the oscilloscope 1 MOhm and 20 pF, cable capacitances and a low-loss 5 nF capacitor. The right branch is called sample branch. Its high-voltage part includes a guarded specimen holder with an impedance $\underline{Z}_s$. The low-voltage side of the right branch $\underline{Z}_{LV2}$ is identical with $\underline{Z}_{LV1}$. Styroflex capacitors were employed due to their low dielectric loss and long-term stability. Surge arresters were connected to inputs of the oscilloscope to protect against overvoltages.

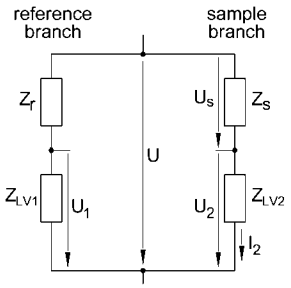

Figure 5.2: Unbalanced bridge circuit for impedance measurement.

For the permittivity measurement, voltage signals were measured on impedances $\underline{Z}_{LV1}$ and $\underline{Z}_{LV2}$ by means of a digital oscilloscope. The raw data was then transmitted to a computer. The measured signal windows of sinusoidal voltages $\underline{U}_1$ and $\underline{U}_2$ were processed into the specimen impedance $\underline{Z}_s$. The result was subsequently corrected with a referencing method (cf. section 5.1.2) in order to accurately determine the magnitude and phase of the impedance $\underline{Z}_s$. Finally, from the specimen impedance calculated from measured values, ε' and ε'' were determined based on the geometrical capacitance.

5.1.2 Referencing

The accuracy of the permittivity measurement, which is particularly crucial for studying low-loss dielectrics, can be enhanced by performing reference measurements on capacitors with well-known capacitances and sufficiently low losses. A brief account of this method is given below.

According to Figure 5.2, the voltage $\underline{U}_1$ multiplied by the dividing ratio of the reference branch gives the total voltage

$$\underline{U} = \frac{\underline{Z}_r + \underline{Z}_{LV1}}{\underline{Z}_{LV1}} \underline{U}_1 \,. \tag{5.1}$$

For the impedance of the specimen, following equation holds

$$\underline{Z}_s = \frac{\underline{U}_s}{\underline{I}_2} = \frac{\underline{U} - \underline{U}_2}{\underline{U}_2} \underline{Z}_{LV2} \,. \tag{5.2}$$

As seen in Equation (5.2), the expression for $\underline{Z}_s$ includes the value of the low-voltage impedance $\underline{Z}_{LV2}$ that depends on frequency and thus contributes an error due to the measurement circuit. This error can be eliminated by taking a reference measurement on a low-loss capacitor with a known impedance $\underline{Z}_s^*$, for which it holds

$$\underline{Z}_s^* = \frac{\underline{U}_s^*}{\underline{U}_2^*} \underline{Z}_{LV2} \,. \tag{5.3}$$

A reference measurement carried out on a low-loss capacitor allows to determine $\underline{Z}_{LV2}$ under conditions close to the measurement on a lossy specimen

$$\underline{Z}_{LV2} = \frac{\underline{U}_2^*}{\underline{U}_s^*} \underline{Z}_s^* \,. \tag{5.4}$$

Figure 5.3 shows the voltage ratios $\underline{U}_2^*/\underline{U}_s^*$ for low-loss Styroflex capacitors. The ratio is not frequency independent. Below 100 Hz

of $\underline{U}_2^*/\underline{U}_s^*$ increases with frequency while the increase rate is higher, the higher the reference capacitance. At low frequencies, the currents flowing through sample and reference branches (Figure 5.2) are very low. The currents were converted to voltage by passive elements $\underline{Z}_{LV1}$ and $\underline{Z}_{LV2}$. This caused systematic errors in the amplitude and phase behaviours of the ratio $\underline{U}_2^*/\underline{U}_s^*$. Ideally, the current/voltage converters $\underline{Z}_{LV1}$ and $\underline{Z}_{LV2}$ should cover a range of logarithmically separated resistances and capacitances to broaden the dynamic range.[68] The influence of lead inductances is visible at higher frequencies, where both the amplitude and phase of the ratio start to increase.

Substituting the expression for $\underline{Z}_{LV2}$ in Equation (5.2) gives the value of the specimen impedance after the elimination of the error due to the circuit

$$\underline{Z}_s = \frac{\underline{U}_s}{\underline{U}_2}\,\frac{\underline{U}_2^*}{\underline{U}_s^*}\,\underline{Z}_s^* \,. \tag{5.5}$$

Equation (5.5) shows that the amplitude and phase of the measured voltage ratio $\underline{U}_s/\underline{U}_2$ are corrected by the factor plotted in Figure 5.3. The amplitude is multiplied by the amplitude of $\underline{U}_2^*/\underline{U}_s^*$, the phase of $\underline{U}_2^*/\underline{U}_s^*$ is subtracted from the measured phase. For this reason, the uncertainty at lower frequencies was greater than in the bulk of the spectrum since the amplitude and phase had to be corrected by larger values (Figure 5.6). The error of permittivity measurement depends on how close the reference impedance $\underline{Z}_s^*$ is to the impedance of the specimen $\underline{Z}_s$ at the given frequency.[68,69] When $\underline{Z}_s^* = \underline{Z}_s$ the phase error is zero. However, in practice it is impossible to create a set of reference capacitors from discrete elements that perfectly match the capacitance of the specimen, which can vary from several ten pF to several nF in one frequency sweep.

In this work, reference measurements were taken in advance on a set of 29 Styroflex capacitors covering the range 80 to 730 pF at

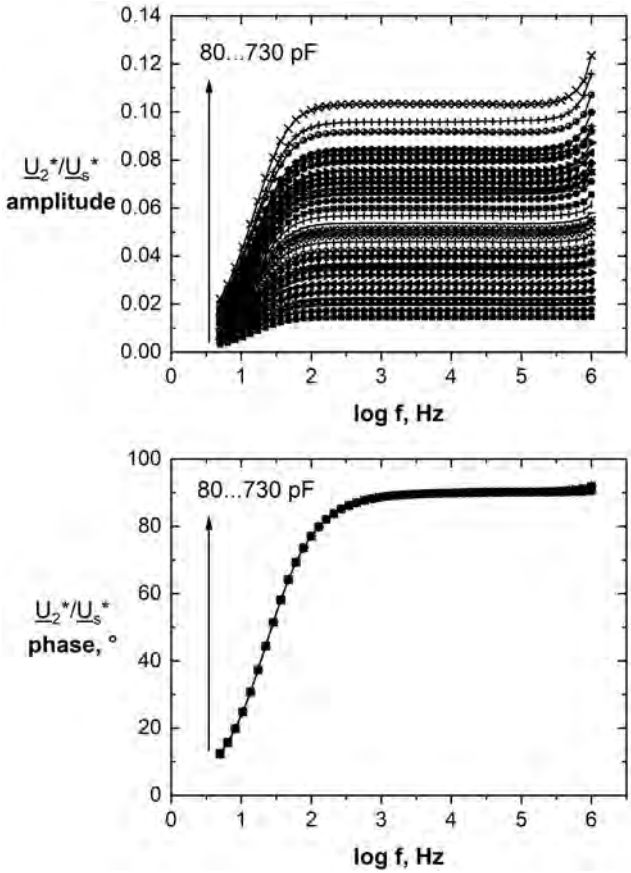

Figure 5.3: Amplitude and phase of the voltage ratio $\underline{U}_2^*/\underline{U}_s^*$ in Equation (5.4) obtained from reference measurements conducted on Styroflex capacitors.

frequencies from 5 Hz to 1 MHz (Figure 5.3). With $\tan\delta < 10^{-4}$ Styroflex capacitors proved to be suitable for use as low-loss references. The capacitances were determined with a calibrated LCR-meter at 1 kHz. The accuracy of the LCR-meter is important, since errors made

in measurements of reference capacitances cause later the uncertainty in the measurement of the permittivity of the specimen. Measuring the capacitance at 1 kHz was a compromise based on the assumption that ε' of the polystyrene remains constant within the considered frequency range. Results of reference measurements were matrices of $\underline{Z}_{LV2}$ with rows corresponding to frequencies and columns corresponding to capacitances. The matrices were saved in a look-up table that was used in the post processing to implement the Equation (5.2).

5.1.3 Signal Measurement and Processing

The complete experimental setup is depicted in Figure 5.4. The equivalent circuit is shown in Figure 5.5. For low-voltage measurements, an arbitrary signal generator Agilent 33250A was used. For high ac-voltage measurements, an ac-source Keysight AC6800-90001 connected to a high-voltage transformer T was employed. The dc-voltage was generated by a manually controlled voltage source with a maximum output voltage of 7.5 kV. The ac-voltage sources were connected to the specimen through a protective capacitance C_{add}. The dc-voltage source was connected to the specimen through a resistor R_{add} to limit the short-circuit current in the event of the specimen breakdown.

The signals $\underline{U}_1$, $\underline{U}_2$ and $\underline{U}_{\text{DC}}$ were measured by means of an 8 bit digital oscilloscope Yokogawa DLM2000 in dc coupling mode. The dc-voltage was measured with a high-voltage probe. Signal windows of varied lengths were saved and transmitted to a computer. The number of periods per signal window varied from 10 to 200 depending on the frequency. The number of measurement points was set to 12500. This resulted in different sampling rates at different frequencies while each period was sampled with 62 to 1250 points. A rather low sampling was chosen to shorten measurement times. The

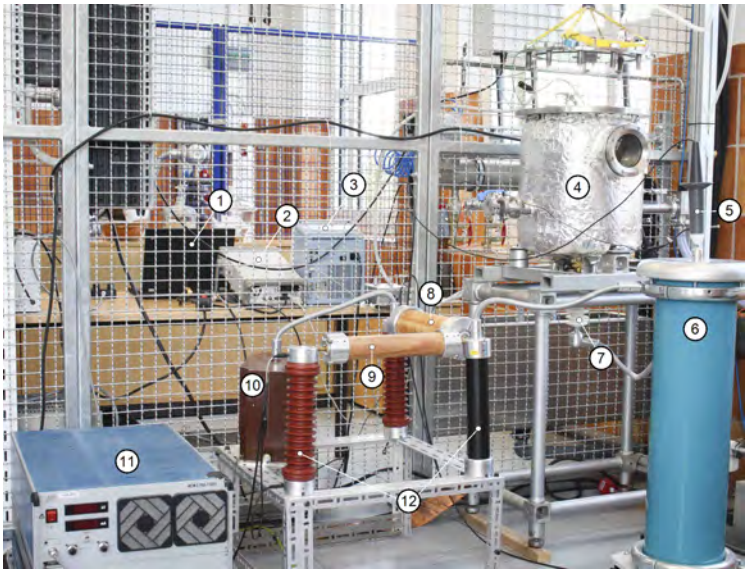

Figure 5.4: Overview of the experimental setup. (1) laptop, (2) function generator, (3) digital oscilloscope, (4) test chamber, (5) high-voltage probe PMK PHV 4002-3, (6) gas-filled capacitor, (7) high-voltage feedthrough, (8) coupling capacitor, (9) protective resistor, (10) high-voltage transformer, (11) dc-voltage source FUG HCP 7500, (12) isolators.

measurement procedure and the signal analysis were controlled by a programme written in MATLAB. Amplitudes and phase angles of $\underline{U}_1$ and $\underline{U}_2$ as well as the dc-voltage U_{DC} were determined by using the Discrete Fourier Transformation (DFT). The DFT returns arrows of amplitudes $A(f)$ and their corresponding phase angles $\Phi(f)$ with the number of elements equal to the sampling rate of measured signals.

$$\begin{aligned} U_1 &= A_1(f_0)\,, & \varphi_1 &= \Phi(f_0)\,, \\ U_2 &= A_2(f_0)\,, & \varphi_2 &= \Phi(f_0)\,, \\ U_{\mathrm{DC}} &= A_3(1)\,. \end{aligned} \tag{5.6}$$

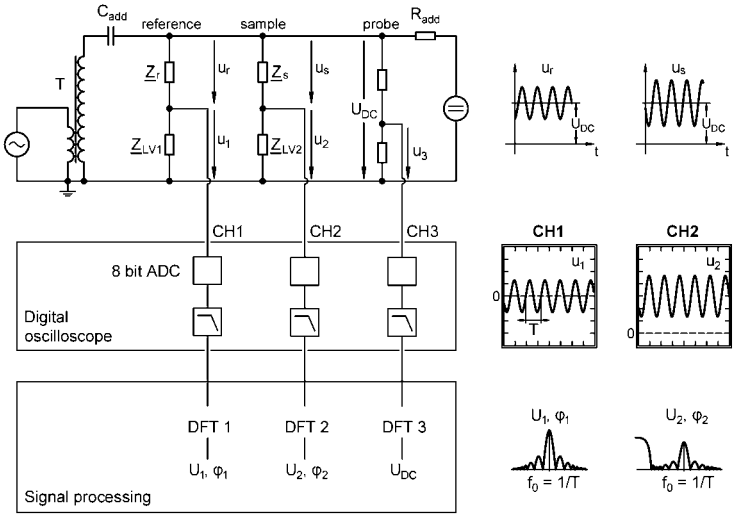

Figure 5.5: The equivalent circuit used in measuring the complex permittivity with an ac-signal superimposed onto a high dc-voltage by means of the unbalanced bridge.

The DFT spectra exhibited a maximum at the fundamental frequency f_0 (Figure 5.5). In conductive specimens, the signal $\underline{U}_2$ featured a significant dc-bias caused by the dc-conductivity of the specimen and the input resistance built in the oscilloscope.

From the known values of U_1 and U_2 and the phase angles φ_1 and φ_2 the specimen impedance was calculated according to Equation (5.5). The real and imaginary components of the complex permittivity were determined from the expression applying for a series

RC-network

$$X_s = \mathrm{Im}(\underline{Z}_s), \qquad C_s = \frac{1}{\omega X_s}, \tag{5.7}$$

$$\delta = \arg(\underline{Z}_s) + \pi/2, \tag{5.8}$$

$$\varepsilon' = \frac{C_s}{C_0}, \tag{5.9}$$

$$\varepsilon'' = \varepsilon' \tan\delta. \tag{5.10}$$

The uncertainty of the sample impedance is determined by the uncertainties of ADCs of the oscilloscope and the uncertainty of the LCR-meter which was used to measure the reference capacitances. The uncertainty in the amplitude measurement of an 8 bit ADC counts 0.39 %. The uncertainty of the LCR meter Newtons4th PSM1735 is specified as 0.1 %. Calculating the combined uncertainty as the root square of the linear sum of squares of each uncertainty for 3 ADCs of the oscilloscope and the LCR-meter gives 0.68 %. The dial gauge used to measure the sample thickess has the accuracy of 4 µm, i.e. 4 % uncertainty for a 100 µm thick foil. Therefore, the uncertainty of ε' is mainly due to the measurement of the thickness of the specimen and electrode surfaces. For this reason, alterations of dielectric properties of different specimens have been compared rather than their absolute values. To assess phase angle and amplitude resolutions, permittivity measurements were made on an air capacitor (Figure 5.6). Guarded electrodes in diameter 40 mm with an electrode separation 75 µm were used. The phase angle determined for air counted less than 10^{-3} rad in the bulk of the spectrum. The deviation of the capacitance remained below 1 %. Due to the phase angle resolution, $\tan\delta$ of low-loss materials like polyethylene could not be sufficiently resolved below 10^{-3}.

To ensure that the application of a high bias field had no influ-

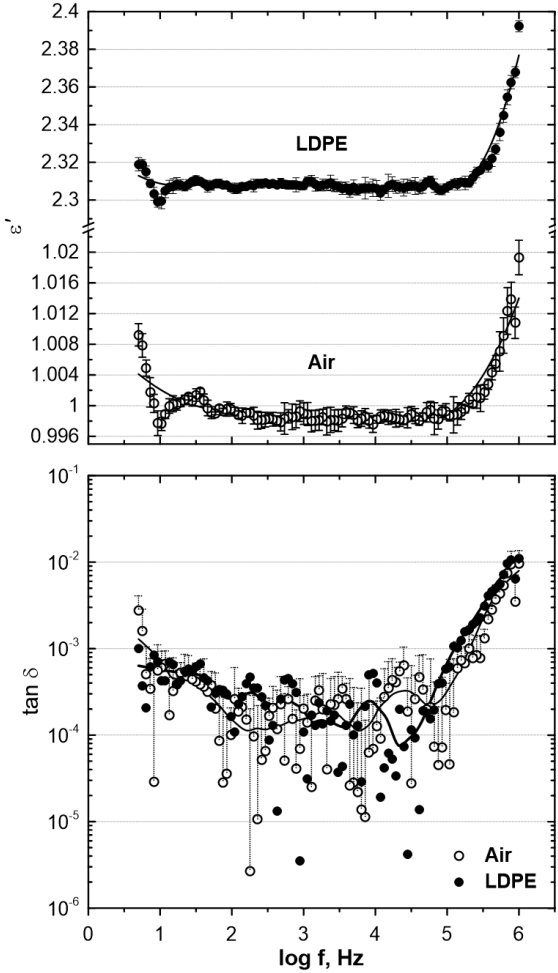

Figure 5.6: Permittivity and loss tangent of an air capacitor made of guarded brass electrodes separated by two 75 µm Kapton spacers and a low-density polyethylene foil in thickness 100 µm with vapour-deposited aluminium electrodes. Data points correspond to means of 5 measurements; error bars depict the doubled standard deviations. The error bars in the bottom graph correspond to measurements on an air capacitor.

ence on the accuracy of measurements, a 100 μm foil of low-density polyethylene (LDPE) was tested at room temperature (Figure 5.7). LDPE was selected due to its low loss tangent and a real part of the permittivity that remains virtually constant in the frequency spectrum of interest. Aluminium electrodes, 40 mm in diameter, were vapour-deposited on both sides. The accuracy both in amplitude and phase resolution were not affected by the applied dc-bias. Scattering of data above 100 kHz was due to the influence of lead inductances at higher frequencies.

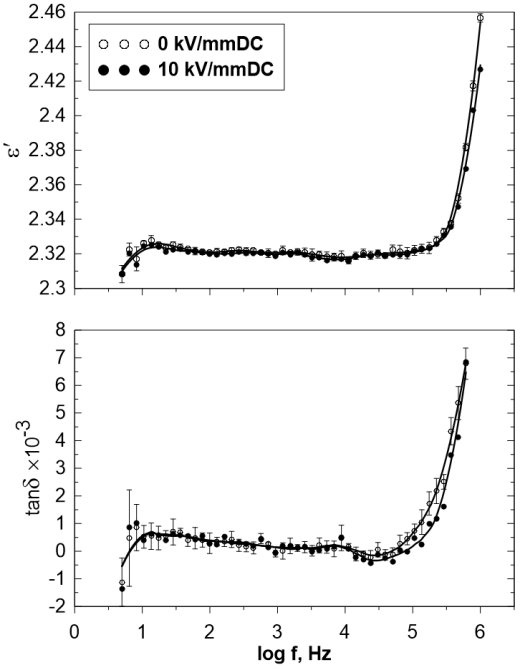

Figure 5.7: Permittivity and loss tangent of low-density polyethylene measured without and with DC voltage superposition.

5.2 Specimen Preparation and Measurement

5.2.1 Specimens

Experiments were carried out on non-impregnated[†] and oil-impregnated papers and Transformerboard manufactured by Weidmann Electrical AG. These materials are widely used in oil-immersed transformers (Table 5.1). Papers made of 100 % cotton fibres were also considered, however the results presented in this work only include materials listed in the table below. Non-impregnated specimens were studied in order to exclude the effects attributable to the oil, although the considered materials are utilised in practice only in combination with an oil impregnant.

Dielectric measurements on non-impregnated papers, especially under application of high voltages, can be associated with extremely high local fields that can distort the measurement through initiating electrical discharges at the surface. The fibrous structure of the paper and the surface roughness of metal electrodes cause a non-uniform electrical contacting. Surface irregularities of an insulating kraft paper or board can reach several micrometers in depth (Figure 5.8). In contrast, the surface roughness R_a of polished brass electrodes was in the range of 0.05 µm. The surface roughness of lapped stainless steel electrodes used in measurements on oil-impregnated units was less than 0.5 µm. At low amplitudes of probing ac-voltages, measurements with an improper contact between the electrodes and the specimen yield a lower permittivity, since on both sides of the specimen, air capacitors act in series. At higher ac-voltages, partial discharges can be initiated causing a drastic increase of the permittivity and loss factor. This is explained through short-circuiting of air capacitors both at the

[†]A non-impregnated paper practically consists of air-impregnated cellulosic fibres. Therefore, in the following text, the terms "non-impregnated" and "air-impregnated" have the same meaning.

Table 5.1: Properties of insulating paper materials adopted from Weidmann product brochures.[70,71]

Grade K pressed paper	
IEC standard:	IEC 60641-3-2, Type P.4.1A
Specimen thicknesses:	100, 240 µm
Raw material:	Sulphate wood pulp
Apparent density:	1.1 g/cm^3
Water content:	< 8 % wt.
Surface:	Light wire marks, smooth
Application:	Layer insulation of oil-immersed transformers
Transformerboard TI	
IEC standard:	IEC 60641-3-1, Type B.2.1
Specimen thicknesses:	200 µm
Raw material:	Unbleached kraft pulp
Apparent density:	1.15 g/cm^3
Water content:	< 8 % wt.
Surface:	Light wire marks, smooth, calendered
Application:	Curved pieces like cylinders with small diameters, punchings, stamped insulation components

surface and in the bulk of the paper.[72] However, the increase of permittivity and loss factor under the application of a high dc-voltage was less pronounced than in the case of high ac-voltage amplitudes. It is presumably due to a lower intensity of discharges that occur less frequently in a smaller volume fraction. A closer examination of contacting methods and their impact on high-field measurements is provided in Section 5.3.

5.2.2 Test Cell

Working with hygroscopic materials, like cellulose, requires a great deal of care during the preparation of specimens and the measurement. Ideally, both steps should take place within the same controlled environment. A heatable vacuum chamber was essential for

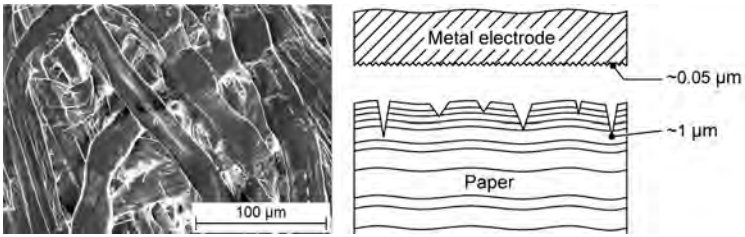

Figure 5.8: Surface structure of the paper (own picture). Schematic of the surface roughness of the metal electrode and paper specimen (right).

conducting experiments on dried paper specimens. The test cell used in the present work was developed on the basis of an existing double-walled vacuum chamber with an inner diameter and the height of 40 cm (Figure 5.9). A 60 kV high-voltage feedthrough in the bottom of the chamber, coaxial signal feedthroughs and thermal elements in the lid were added to enable high-voltage measurements. On the outer wall a 10 m long heating cord was attached. The space between the two walls was filled with a heat-resistant silicone oil to increase the thermal conduction. The temperature in the chamber was regulated by two PID controllers with temperature reads on the inner and outer walls of the chamber. The temperature of the electrode arrangement was measured with a thermal element inserted into the guard ring. It could be elevated up to 130°C. The pressure in the cell was measured with a combined capacitive and Pirani vacuum meter. Vacuum pressure of $5 \cdot 10^{-2}$ mbar could be reached with a rotary vane pump. The specimens were impregnated under vacuum with oil, injected through a needle valve in the lid of the chamber. To prevent the hydration of thoroughly dried specimens, the chamber was filled with dry air and molecular sieve was placed on the bottom.

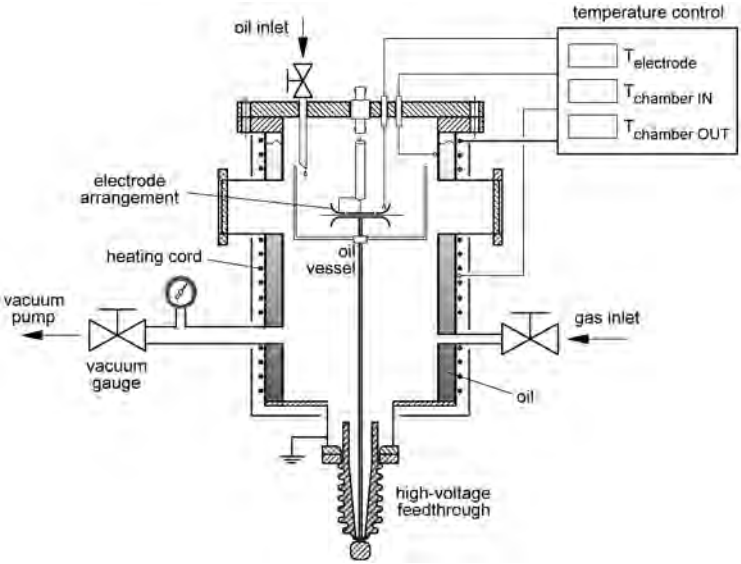

Figure 5.9: Test cell for preparation of specimens and dielectric measurements.

5.2.3 Oil Conditioning

Paper specimens were impregnated with dried and degassed mineral oil. The self-developed glass apparatus for drying and degassing of oils is illustrated in Figure 5.10. Compared to paper, water dissolved in oil can be removed much easier in vacuum when heating the oil and increasing the contact surface with the atmosphere. The developed system ensures all three conditions at the same time. The fresh oil is drawn into the drying column, which is under vacuum of 1 mbar. The flow rate is regulated with a valve and glass filters. The water jacket heated to 50°C maintains a constant temperature of the internal tube. The special internal structure of the drying column increases the contact surface of oil with the ambient atmosphere. The dried and de-

gassed oil drops into a Woulff bottle. With this method, mineral oils can be dried down to 2 ppm_w.

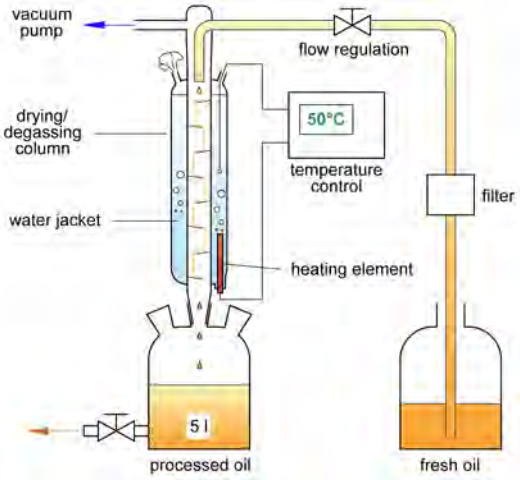

Figure 5.10: System for drying and degassing of oil.

5.2.4 Preparation of Specimens

For non-impregnated specimens, three different degrees of hydration were considered: 1) untreated units with 6 – 8% wt. water, 2) moderately dried units with about 4 % wt. and 3) thoroughly dried units with less than 0.5% wt. water. Specimens with the lowest water content were dried under vacuum at 120°C for at least 24 hours and stored in a desiccator filled with molecular sieve. Although the specimens were shortly exposed to the ambient atmosphere while placing them into the specimen holder, the water content after the measurement counted less than 0.5 % wt. Moderately dried units were either dried for 24 h in an oven at 50°C under normal atmosphere or stored in a desiccator with a little amount of desiccant for at least one week.

Part of specimens was impregnated with vacuum treated mineral oil Shell Diala S4 ZX-1. A measuring cup with specimens was placed into the test chamber and subjected to vacuum of $5 \cdot 10^{-2}$ mbar. Figure 5.11 shows the internal of the test chamber prepared for the impregnation. The impregnation took place at room temperature with oil warmed up to 40 – 45°C. The oil was drawn in through a needle valve and a silicone tube. An effective reduction of the water content of oil-impregnated specimens was achieved by adding molecular sieve into the measuring cup. Specimens with a higher degree of hydration were impregnated without previous drying under vacuum.

5.2.5 Measurement of the Water Content

The water content in the paper was determined by means of a Karl-Fischer coulometry.[73] A coulometer METROHM Model 652 KF with a heating unit 707 KF oven was used. The non-impregnated specimens were heated to 200°C in the drying unit under N_2-flow of 100 ml/min. The extracted water is thereby transported into the anolyte. In the coulometric water determination, iodine is generated automatically from the iodide containing electrolyte through the anodic oxidation. The coulometer measures the current flowing through the anolyte and the time required to achieve the endpoint of the titration. The electric charge, determined as the product of the current and time, quantifies the amount of the consumed iodine which is directly proportional to the amount of water added to the anolyte. The water content of oil-impregnated specimens was determined through methanol extraction. Oil-impregnated snippets were mixed in methanol with a known water content. The methanol-water mixture was then added directly to the anolyte.

The water content of the oil was measured with a capacitive moisture sensor made by E+E Electronics. The sensor incorporates

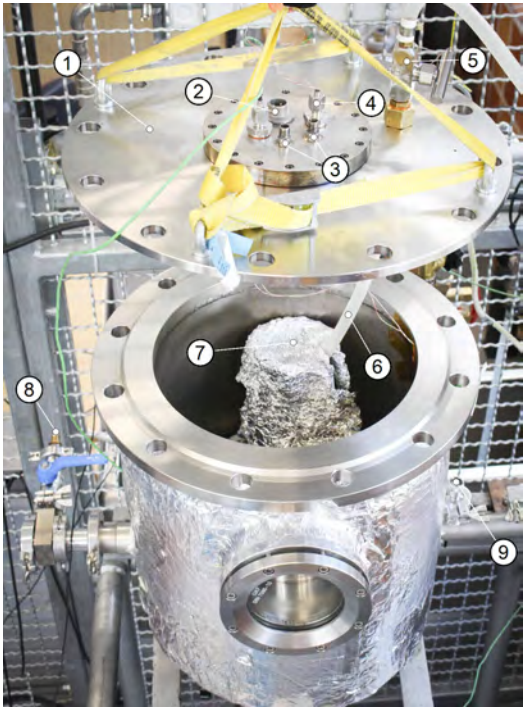

Figure 5.11: Test cell arranged for impregnation of paper specimens. (1) liftable lid of the vacuum chamber, (2) electrical feedthrough, (3) coaxial feedthroughs, (4) fittings for thermal elements, (5) needle valve for oil inlet, (6) silicone tube for oil inflow, (7) measuring cup with specimens, (8) ball valve for gas inlet, (9) ventilation valve.

a thin film of a water active polymer that absorbs or releases water depending on the moisture content of the liquid. The amount of moisture present in the liquid is determined from the capacitance of the sensor. Oil molecules or its other components cannot penetrate into the polymer film.

5.2.6 Specimen Holders

The specimen holder for non-impregnated specimens (Figure 5.12 and 5.13-a) consists of an aluminium frame with a Teflon insulation separating the high-voltage electrode **I** from the frame **D**. The electrodes were made of machined brass with mirror-polished measuring surfaces. The outer edges of the high-voltage and guard-electrodes were rounded off by 5 mm. The bottom electrode is moved in axial

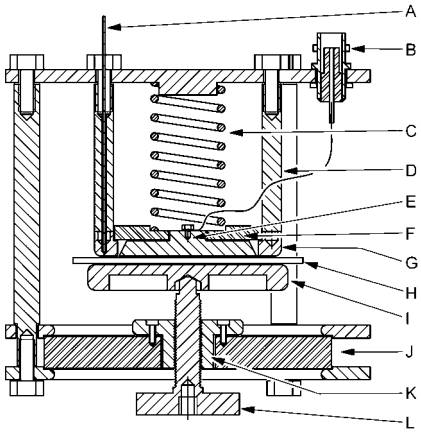

Figure 5.12: Schematic drawing of the specimen holder. **A** – thermal element type K, **B** – coaxial connector, **C** – spring, **D** – aluminium frame, **E** – measuring electrode, **F** – Teflon centering disk, **G** – guard electrode, **H** – specimen, **I** – high-voltage electrode, **J** – Teflon insulator, **K** – flanged nut, **L** – tightening screw.

direction by means of a fine thread screw **L** that eased the insertion and positioning of the specimen. The adjusting screw has a threaded hole in the bottom for a secure placement of the specimen holder inside the test cell. The diameter of the measuring electrode **E** is 40 mm. It is loaded by an iron spring that was intended to maintain a uniform pressure of 20 kPa in the clamped state. The spring is isolated from the measuring electrode by a Teflon plate **F**. A coaxial connector **B** is mounted on the top plate of the frame. A temperature sensor

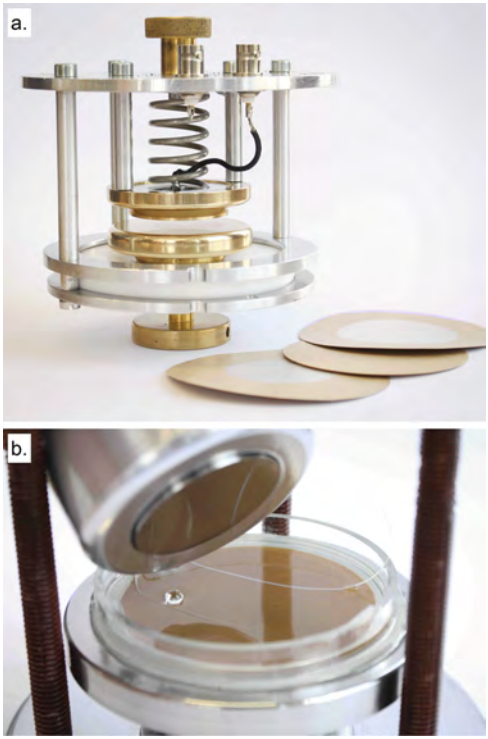

Figure 5.13: Specimen holders: (a) for non-impregnated specimens, (b) for oil-impregnated specimens. Teflon spacers are shown.

A was attached to the guard electrode through a hole in one of the supporting rods of the aluminium frame. The specimen holder for oil-impregnated units consists of a high-voltage electrode with a glass ring glued on it and a guarded measurement electrode with a diameter of 40 mm (Figure 5.13-b). Both electrodes were made of stainless steel 1.4301. In measurements on oil-impregnated units, 20 kPa load was applied to the measuring electrode with a metal spring. In measurements on oil-paper layered specimens, the measuring electrode rested on Teflon spacers without additional pressure.

5.3 Effect of the Electrode-Specimen Interface

The international standard for the measurement of dielectric properties of insulating papers IEC 60554-2[74] only specifies 20 kPa as a mechanical load on measuring electrodes that is required for a sufficient electrical contact. Use of conductive paint or evaporated electrodes is not mentioned. In references on dielectric spectroscopy of cellulosic materials, there is a certain arbitrariness in this concern. In some works metal plates were pressed onto fibrous or powder based specimens by applying large pressures up to 1900 bar.[63] Other authors opted for evaporating the electrodes directly onto the specimens.[75]

Considering the microscopic surface topography of the cellulosic paper (Figure 3.1 on page 16) it is reasonable to evaluate different methods of electrical contacting, e. g. mechanically pressed bare electrodes, aluminium evaporation, conductive paint etc. The surface of a fibrous paper is naturally covered by cracks and pores. The pores typically reach several microns in depth. As mentioned earlier, when contacting the paper with machined metal electrodes, air pockets remaining in the interspace can hamper the measurement of the permittivity, by acting as air capacitors (Figure 5.8). This issue can be

eliminated by employing evaporated or painted electrodes. While for polymers like polyethylene several tens of nanometers provide a sufficiently conductive layer, several hundreds of nanometers need to be deposited onto a cellulosic paper to reach a comparable conductivity (Figure 5.14-a). At a closer magnification it can be seen, how metal particles coat the fibres, exactly following the surface irregularities. In this work, conductive silver paint was used as a faster and cheaper alternative to the metal evaporation. The paint consisted of particles that did not penetrate into the volume of paper. The microscopic views from top and from the side show a layer of silver in thickness around 5 µm (Figure 5.14-b and 5.15) that consists of flat particles. As seen in the cross-section, the silver coating creates a layer that also follows the structure of the paper, although not as good as the aluminium evaporation.

Besides lowering the permittivity of the specimen, the presence of air pockets critically increases the electric field at the electrode-specimen interspace leading to partial discharges. A simple calculation of the dc potential distribution around a surface roughness that is represented by a semi-circular air pocket reveals notable differences between uncoated, coated or oil-impregnated specimens (cf. Figure

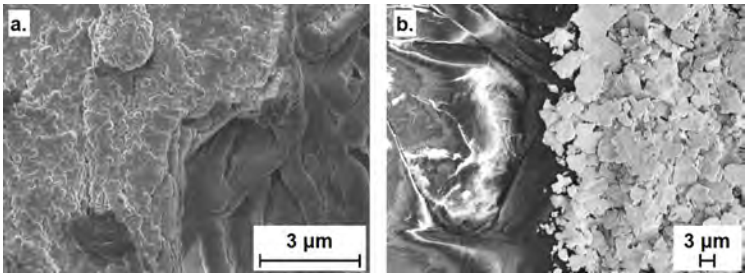

Figure 5.14: Surface of the paper specimen with a conductive coating: (a) aluminium evaporation, (b) silver paint.

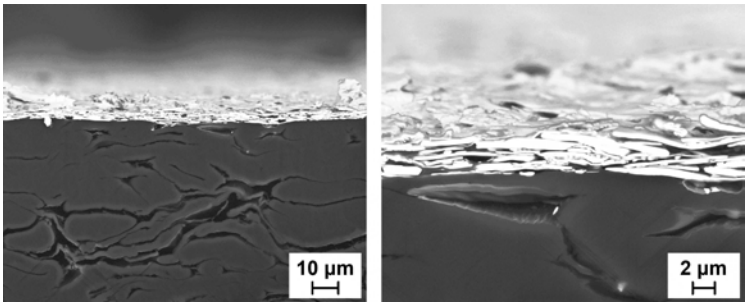

Figure 5.15: The cross section of the insulating paper painted with conductive silver paint. The sample was prepared with ion beam slope cutting with Leica EM RES102.

5.16). If the surface is uncoated, the electric field is displaced into the air pocket (cf. Figure 5.16-a). Large field intensities arise at contact points between the electrode and paper. This is indicated by the highest density of equipotential lines at the corners of the semi-circle. If the surface is metallised through aluminium evaporation or with silver paint, the field maximum arises at the deepest point of the roughness (cf. Figure 5.16-b). Impregnation with oil also reduces the field at triple points according to the conductivity ratio of oil and paper. Figure 5.16-c illustrates the field distribution when the conductivity ratio between oil and paper is assumed 100. The electric field in a system of a more conductive cellulose and less conductive oil would be rather concentrated in the oil filled inclusion similar to Figure 5.16-a. The conclusion is that, under a dc-field, due to the irregular surface of the paper, electric fields much higher than the net field occur along the boundary between the paper and the electrodes. Impregnation with oil and a metallic coating reduce the field strength in the vicinity of electrodes at the same time displacing the field maximum into the depths of surface irregularities.

The role of the electrical contacting was examined by compar-

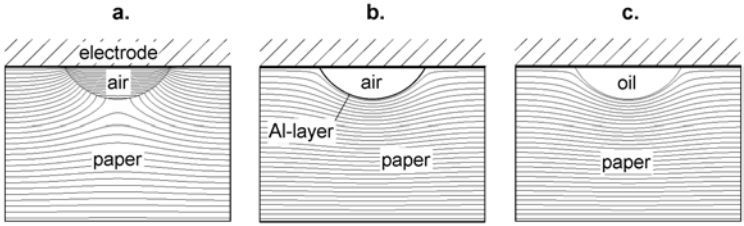

Figure 5.16: Equipotential lines of the static voltage around a surface void of paper: (a) non-impregnated paper without conductive coating $\varepsilon_{\text{paper}}/\varepsilon_{\text{air}} = 6$, (b) non-impregnated paper with conductive coating, (c) oil-impregnated paper without coating, assumed relation of material parameters $\sigma_{\text{oil}}/\sigma_{\text{paper}} = 100$, $\varepsilon_{\text{oil}}/\varepsilon_{\text{paper}} = 0.5$.

ing the frequency spectra of $\tan\delta$ measured with different contacting methods (Figure 5.17). The spectra were measured with a low-voltage ac-signal with zero bias (filled squares) and with a dc-bias of 6.75 kV/mm (empty squares). The brass electrodes were pressed onto the specimen with a constant pressure of 20 kPa. Conductive layers, including silver paint, tin, gold, or conductive rubber were applied onto the specimen before placing it between the electrodes. A round piece of conductive rubber of the same diameter as the measuring electrode (Figure 5.12) was placed between the brass electrode and the paper. The main differences were observed in $\tan\delta$ measured at a superimposed bias field.

Uncoated specimens featured a distinct relaxation peak arising between 100 Hz and 1 kHz due to the bias field (a - c). Compared to bare metal electrodes, a more pronounced peak was found when using conductive rubber (b). It seems, that the rough surface of the rubber which is in contact with a similarly rough surface of the paper, leads to even higher microscopic electric fields than in the case of mirror-polished metal electrodes. Almost no changes due to the bias field were observed when coating the specimens with conductive sil-

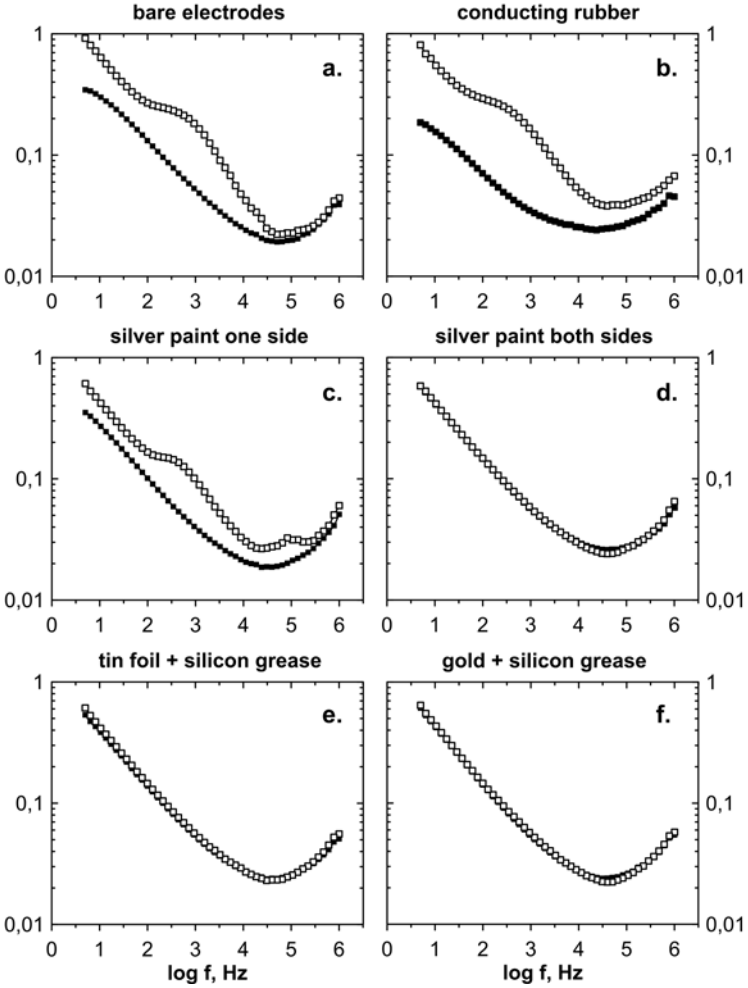

Figure 5.17: Loss tangent spectra of a non-impregnated Transformerboard in thickness 0.2 mm with 7.5 ± 0.5 % wt. moisture measured at 24°C with different contacting methods. Filled squares correspond to an unbiased sinusoidal excitation, empty squares correspond to sweeps with a dc-bias of 6.75 kV/mm.

ver, tin or gold foil (d - f). Tin and gold foils were applied by means of a thin layer of silicon grease. Interestingly, the peak in $\tan\delta$ was of lower magnitude in the specimen painted with silver on one side and contacted with a bare electrode on the other side (c). This might be explained by the fact that the area at which high electric fields cause the ionisation is smaller than in cases (a) and (b). Silver paint electrodes seem to create conductive layers on the surface of the paper akin to metal evaporation (Figure 5.15). Therefore, extremely high local fields do not occur at the surface as in the case of bare electrodes. Thin layers of silicon grease, used as an adhesive for applying tin or gold foils, even up the surface of the paper and thereby prevent electric field concentrations (cf. Figure 5.16).

5.3.1 Conclusion

Dielectric properties of non-impregnated cellulosic papers were found to be strongly dependent on the electrical contacting. In low-field measurements, the air remaining between the specimen and electrodes reduces the value of ε' and shifts the relaxation peaks in ε'' to higher frequencies (cf. curves a and d in Figure 5.17). In high-field measurements, due to the poor electrical contacting, extremely high local fields arise at the surface of the specimen. In the spectrum of ε'' or $\tan\delta$, a distinct relaxation peak occurs under the influence of a high bias field. It is suggested, that electrical discharges at points of high field concentrations lead to the ionisation. The occurrence of free ions is detected with the dielectric measurement in form of a new relaxation peak.

6 Results

The first part of the present chapter reports measurements carried out on non-impregnated papers. The second part presents results obtained on oil-impregnated papers. The description follows the chronological order in which the experiments were completed.

6.1 Time-Resolved Measurement

The time-resolved measurement of the permittivity and loss tangent was done to observe the possible alterations of dielectric properties due to the bias field over the course of several hours. Non-impregnated Transformerboard specimens with 8 % wt. and less than 0.2 % wt. moisture were studied. The specimens were not covered with conductive coating and were placed between metal electrodes under a spring tension of 20 kPa. Measurements were taken at constant frequencies of the low-amplitude ac-voltage of 50, 500 Hz and 10 kHz. It was expected that the most pronounced alterations of ε' and $\tan\delta$ would be observed at 50 Hz in wet specimens, since their permittivity and loss tangent increased towards lower frequencies due to slower relaxation mechanisms. Figure 6.1 shows relative alterations of ε' and $\tan\delta$ determined as

$$\Delta \tan\delta_{\mathrm{rel}} = (\tan\delta_i - \tan\delta_0)/\tan\delta_0 \cdot 100\%\,, \tag{6.1}$$

$$\Delta \varepsilon'_{\mathrm{rel}} = (\varepsilon'_i - \varepsilon'_0)/\varepsilon'_0 \cdot 100\%\,, \tag{6.2}$$

where $\tan\delta_0$ and ε'_0 correspond to initial values before the bias field application.[76]

In fact, the permittivity and loss tangent of wet specimens increased instantaneously upon the application of a bias field and no alterations were found in well-dried units. However, the highest relative

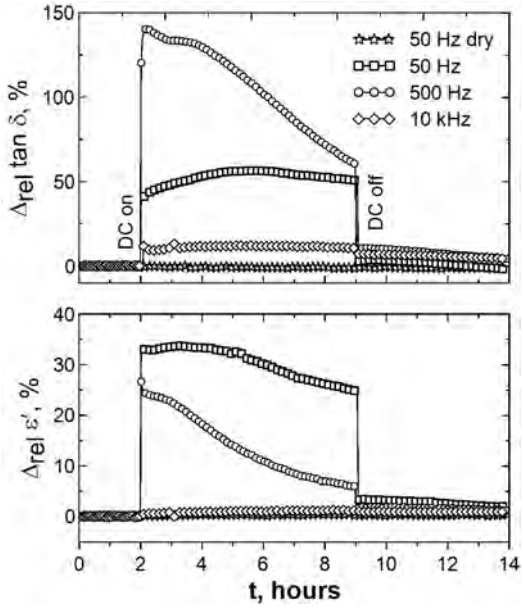

Figure 6.1: Time-dependence of relative changes of ε' and $\tan\delta$ of Transformerboard measured at 20°C and water content 8.2 % wt. and less than 0.2 % wt. The moments when the dc-field of 2.3 kV/mm was applied and removed are indicated.

change and the fastest development of $\tan\delta$ was observed at 500 Hz instead of 50 Hz. No steady-state values of ε' and $\tan\delta$ could be measured even after maintaining the bias field for 7 hours. Upon the removal of the dc-field, ε' and $\tan\delta$ slowly decreased to their original values identifying small remaining changes.

Measurements carried out at 50°C on equally wet specimens showed faster alterations of ε' and $\tan\delta$ under the action of the bias field. (Figure 6.2). However, due to the temperature, a gradual removal of water appreciably lowered the permittivity and loss tangent even before the dc-field was applied. The drop of the water content

from 8.2 % wt. before to 7.3 % wt. after the measurement supports this assumption. The decrease of ε' and $\tan\delta$ due to drying was better visible at 50 Hz, which is closer to the peak of β_{wet}-relaxation peak. Yet, compared to room temperature, ε' and $\tan\delta$ changed faster at 50°C under the action of the bias field.

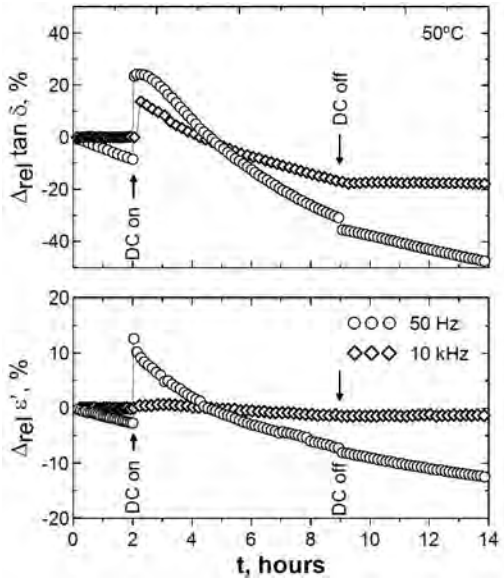

Figure 6.2: Time-dependence of the dielectric properties of Transformerboard measured at 50°C and water content 8.2 % wt. before and 7.3 % wt. after the measurement. The moments when the dc-field of 2.3 kV/mm was applied and removed are marked with arrows.

6.2 Variation of Components of the Mixed Field

Preliminary measurements on hydrated insulating papers, in which the bias field was elevated in steps, revealed a marked nonlinear behaviour of both parts of the complex permittivity.[76] The shape

of curves $\varepsilon'(E_{\mathrm{DC}})$ and $\varepsilon''(E_{\mathrm{DC}})$ and their total increase depended on the frequency of the probing ac-voltage. The relative increase of the loss factor ε'' featured a maximum at 100 Hz. For this reason, measurements at a varying bias field were carried out at 100 Hz. Below, experimental details are discussed and the influence of the amplitude of the probing ac-voltage on the complex permittivity is analysed. Results were complemented with tests conducted on materials with dielectric properties less sensitive to the bias field. For a faithful comparison, the effect of the bias field is presented in terms of absolute changes $\Delta\varepsilon' = \varepsilon'_{\mathrm{dc}} - \varepsilon'_0$ and $\Delta\varepsilon'' = \varepsilon''_{\mathrm{dc}} - \varepsilon''_0$, where $\varepsilon'_{\mathrm{dc}}$ and $\varepsilon''_{\mathrm{dc}}$ are values measured with a biased ac-voltage, and ε'_0 and ε''_0 are measured at zero dc-bias.

Since the complex permittivity was measured 30 seconds after each ramping of the bias field, they cannot be considered as steady-state values. In fact, as shown in Figure 6.3, ε' and ε'' start to decay upon increasing the bias field. The decay was stronger when measuring with a low-amplitude ac-voltage especially in the region where the permittivity rapidly increased with the dc-field. Furthermore, as observed in time-resolved measurements, (Figure 6.1), the time-dependent change of the permittivity may distort the measurement at higher dc-voltages, since the higher the dc-voltage, the longer has the specimen been hitherto stressed. Measuring the permittivity 30 seconds after ramping the bias field was therefore a compromise that resulted in a steeper increase of $\Delta\varepsilon'(E_{\mathrm{DC}})$ and $\Delta\varepsilon''(E_{\mathrm{DC}})$, than if the points were measured in the steady-state.

The increase of ε' and ε'' caused by the bias field depended on the degree of hydration. The highest alterations were observed in room-humid specimens with 7.2 % wt. water tested with a low-amplitude ac-voltage (Figure 6.4). With the increasing bias field, ε' and ε'' increased and eventually reached a plateau. The slope up to the

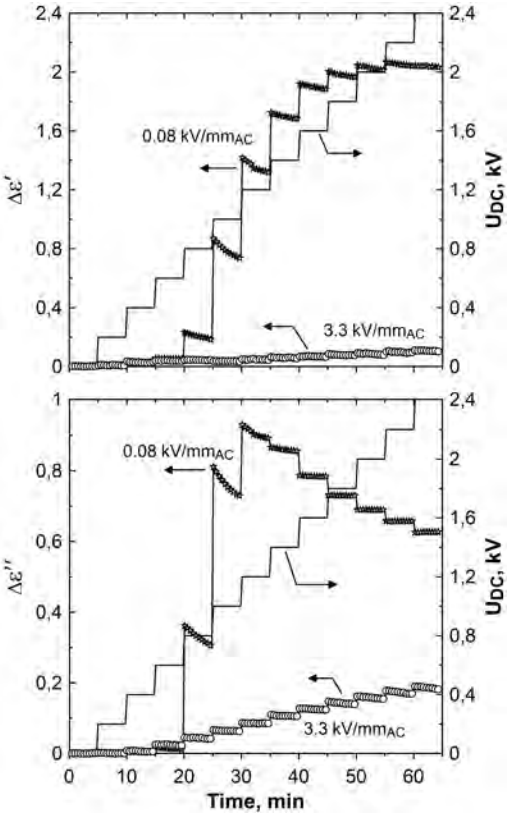

Figure 6.3: Absolute increase of ε' and ε'' of a cellulosic insulating paper Grade K in thickness 240 µm (7.2 % wt. water) due to a stepwise elevation of the superimposed dc-bias, measured with a low and high amplitude ac-voltage of 100 Hz at 23°C.

plateau was lower at higher amplitudes of the probing ac-signal. At a further elevation of the bias field, ε' and ε'' of hydrated specimens started to decrease, followed by an imminent breakdown. In dry specimens, measurable alterations were observed only in ε'. This applied also for PTFE contacted with bare electrodes. On the other hand, ε'

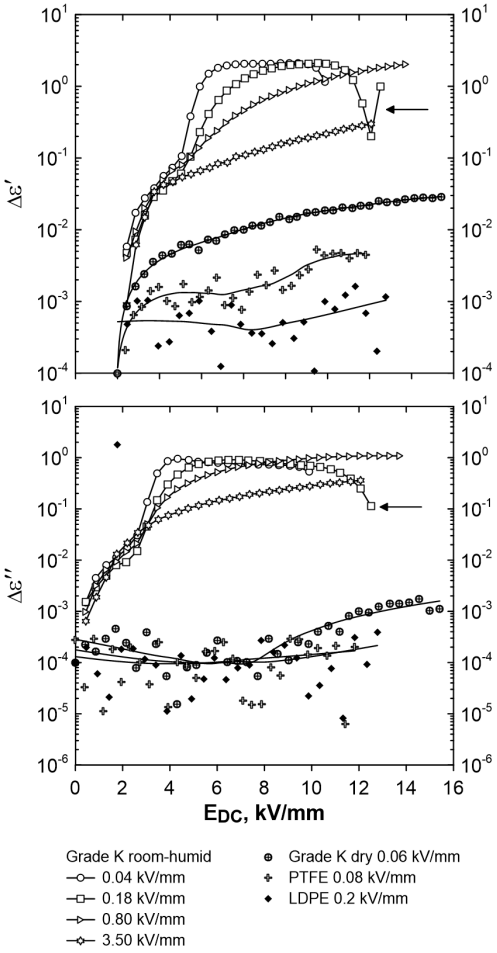

Figure 6.4: Absolute increase of ε' and ε'' of different materials due to the superimposed dc-field at 23°C. Water content of the room-humid Grade K paper 7.2 % wt., dried Grade K paper < 0.5 % wt. Peak values of the probing ac-field are given. Arrows indicate the moment before breakdown.

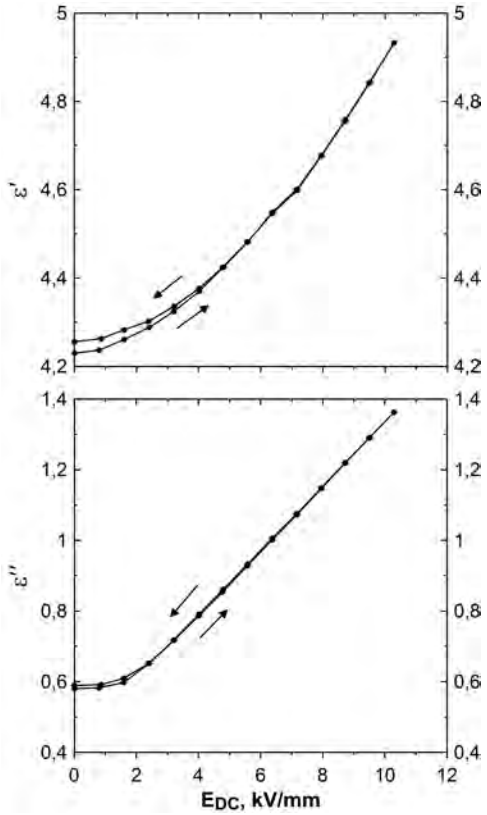

Figure 6.5: Real and imaginary parts of the complex permittivity of a room-humid insulating paper Grade K as function of the dc-field. Measured at 23°C by superimposing a probing ac-voltage resulting in 3.5 kV/mm.

and ε'' of polyethylene with vapour-deposited aluminium electrodes remained virtually constant.

Gradual decrease of the bias field caused minor hysteresis-like effects (Figure 6.5). ε' and ε'' at the end were slightly higher than in the pristine state. However, the observation was rather inconsistent for

different papers and depended on the overall duration of the bias field application.

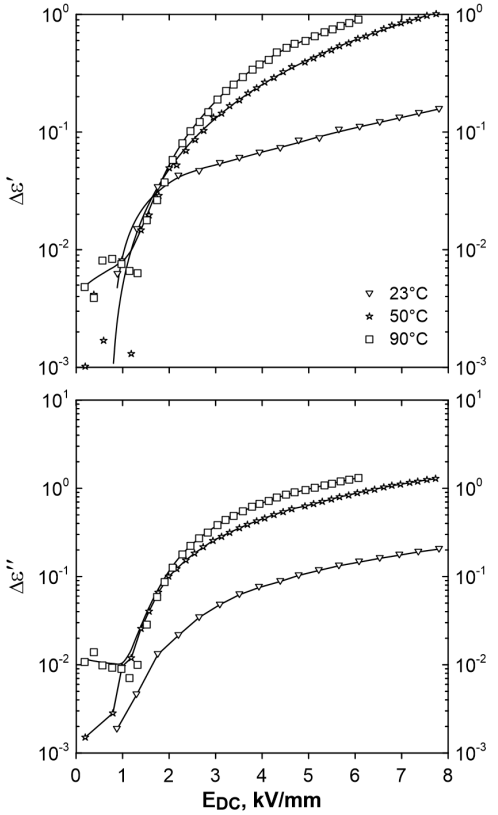

Figure 6.6: Absolute increase of ε' and ε'' of a non-impregnated Grade K insulating paper with 7 – 8 % wt. moisture at different temperatures.

The effect of the bias field was stronger at higher temperature (Figure 6.6). As seen earlier, the water content of wet paper clamped between metal electrodes decreases even at moderate increase of temperature. This is reflected in changes of ε' and ε''. Maintaining a con-

stant water content during the measurement was difficult. Therefore results shown in Figure 6.6 give only a qualitative comparison.

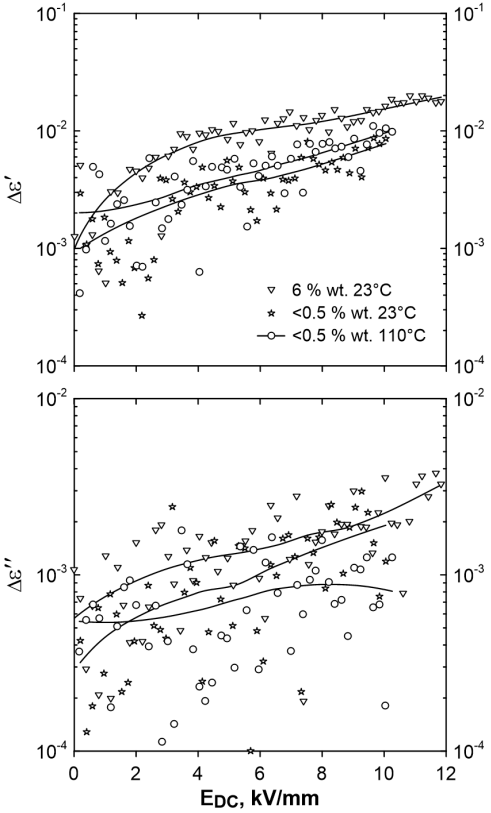

Figure 6.7: Absolute increase of ε' and ε'' of a non-impregnated Grade K insulating paper contacted with silver paint electrodes at different water contents. The peak value of the probing ac-field was 3.5 kV/mm.

Measurements on low-loss polymers have indicated the importance of a proper electrical contacting. For paper specimens, silver paint electrodes were used as a simple alternative to metal evapora-

tion. Besides silver particles the silver paint contains organic solvents. Their impact on the dielectric properties of papers was not analysed in the present work. Painted specimens were stored in a desiccator for at least one hour for the solvent to dry. Results obtained with silver paint electrodes suggest that the previously mentioned anomalous increase of dielectric properties is due to the electrical contacting (Figure 6.7). The permittivity increase of silver coated specimens was much lower compared to uncoated units. Similar to previous results, the hydration caused slightly higher $\Delta\varepsilon'$ and $\Delta\varepsilon''$. Thoroughly dried specimens were tested at a higher temperature. It was expected that the increase of the ionic mobility would enhance the dielectric properties. However, no substantial difference was noticed between room and high temperature. In both measurements, the enhancement of ε' was in the range of 10^{-2} at a bias field elevation up to 10 kV/m.

6.3 Effect of the Bias-Field on Frequency Spectra

By means of dielectric spectroscopy employing a low-amplitude ac-signal superimposed onto a high bias field, it was intended to verify the previous observations and to elucidate the alterations of ε' and ε'' by ascribing them to relaxation mechanisms of cellulose. The approach was to compare the dielectric spectra measured in the presence of a bias field with spectra measured with an unbiased ac-signal.

The loss tangent spectra graphed in Figure 6.8 were measured on a pristine Grade K insulating paper before applying the bias field, and once in an hour at a maintained bias field of 10 kV/mm as well as immediately after the field removal. Measurement of one spectrum took less than a minute. The field and time dependent changes of dielectric properties within this time were small enough such that each spectrum can be regarded as an instantaneous state. The effect of the

dc-field application to a wet specimen was marked by a distinct loss peak occurring at around 100 Hz and an increase of the permittivity at lower frequencies. The peak appeared upon the application of a dc-field and slowly faded within several hours at a maintained stress.

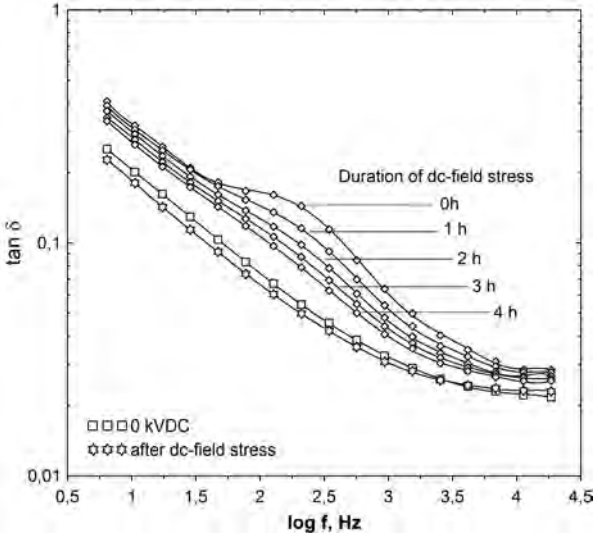

Figure 6.8: Frequency spectra of the loss tangent of a room-humid cellulose paper under a dc-field stress of 10 kV/mm applied for 4 hours. Measured at 20°C.

The loss peak emerged gradually with the increasing bias field (Figure 6.9). While the magnitude of the peak reached a plateau, the frequency of the loss maximum shifted to higher frequencies. The cut plane at 127 Hz in the inserts shows, what causes the s-shaped dependence of ε' and ε'' on the bias field (cf. Figure 6.4). From a visual examination of dielectric modulus $M''(\omega)$ one can assume that the peak of concern originates from the water induced β_{wet}-relaxation and moves down the high frequency shoulder of the β_{wet}-peak. The dielectric modulus is the reciprocal of the complex permittivity $M^*(\omega) =$

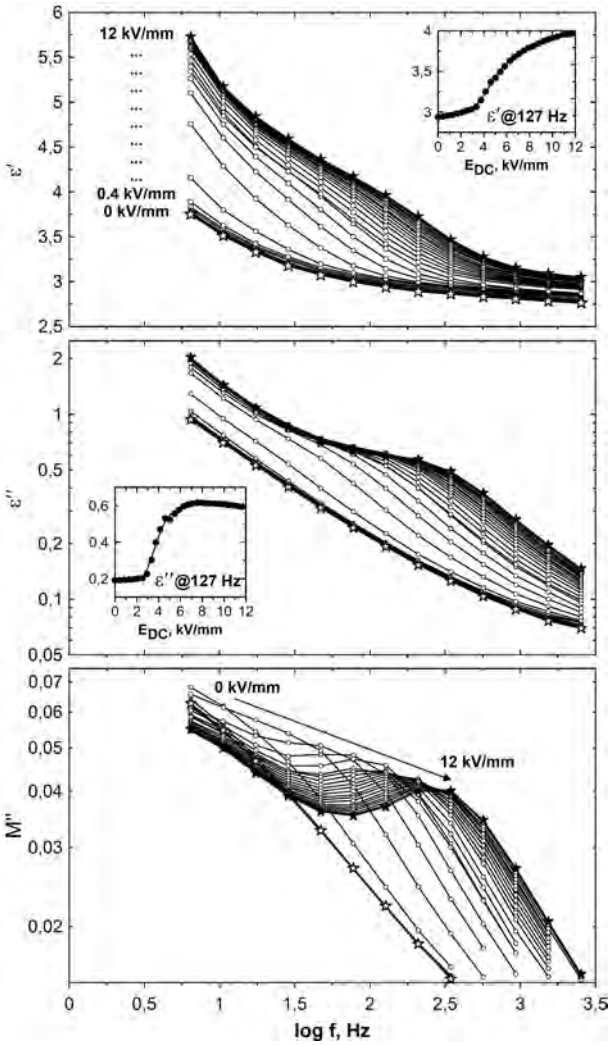

Figure 6.9: Spectra of the real and imaginary parts of the complex permittivity and imaginary dielectric modulus measured immediately after applying different bias fields on an insulating paper with 7 % wt. moisture at 20°C.

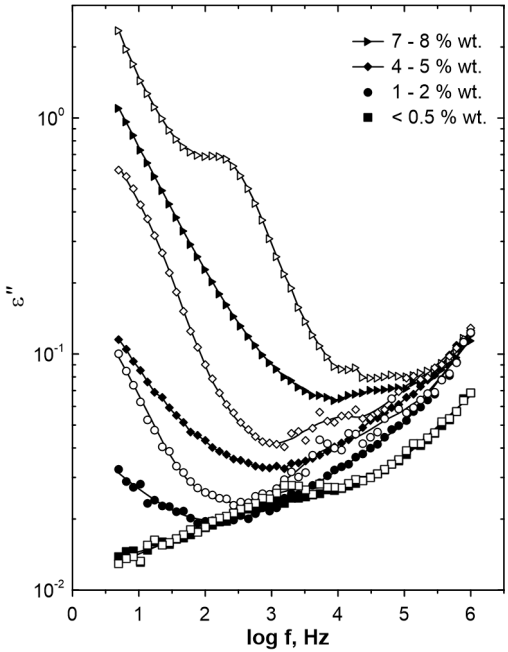

Figure 6.10: Dielectric loss spectra of an insulating paper Grade K measured at different water contents at 20°C. Filled symbols were measured with an unbiased ac-signal, empty symbols were measured under a bias field of 8 kV/mm.

$1/\varepsilon^*(\omega)$. In the $M''(\omega)$ plot, the loss peaks appear at higher frequencies than corresponding loss peaks of $\varepsilon(\omega)$ which is a useful feature if the frequency spectrum is restricted. A slope in $\varepsilon''(\omega)$ is transformed to a peak in modulus representation.

Variation of the water content supported the assumption, that the dielectric relaxation arising due to the bias field is related to the β_{wet}-relaxation (Figure 6.10). As for results of measurements with an unbiased ac-signal, the increase of the water content was associated with the increase of the dielectric loss on the low-frequency side, i.

e. the emergence of the β_{wet}-relaxation peak (cf. Figure 4.8). Under the action of a bias field, both ε' and ε'' increased at lower frequencies depending on the degree of hydration. Even at moderate amounts of water, a distinct relaxation peak shaped at lower frequencies that moved to higher frequencies with the increasing water content similar to the β_{wet}-peak. The peak appeared in the observed frequency region at 4 – 5 % wt. moisture. It featured a sharper peak compared to the β_{wet}-relaxation. In the range between 1 kHz and 100 kHz, ε' and ε'' scattered in presence of a bias field, implying a distortion through discharges occurring at the surface of the uncoated specimen.

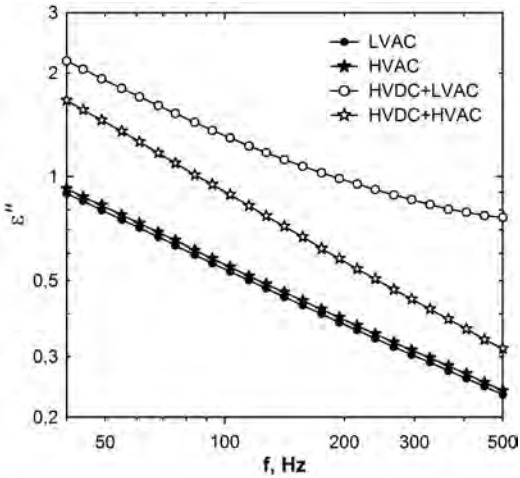

Figure 6.11: ε'' of an insulating paper with 7 – 8 % wt. moisture at 20°C. The bias field $E_{HVDC} = 7.3$ kV/mm, peak electric field due to the low ac-signal $E_{LVAC} = 0.04$ kV/mm, peak electric field due to the high ac-signal $E_{HVAC} = 3.3$ kV/mm.

Smaller alterations of the permittivity without a loss-peak occurrence were measured when superposing a high-amplitude ac-signal onto a dc-bias (Figure 6.11). This is in agreement with observations

from the preceding subsection (cf. Figure 6.4). Mainly the low-frequency part of the loss spectrum was influenced by the dc-field when a high ac-voltage was acting. The slope $\varepsilon''(f)$ increases upon applying the bias field.

6.3.1 Hidden Relaxation Peaks

The logarithmic derivative $\varepsilon''_{\mathrm{der}} = -\partial\varepsilon'/\partial\ln\omega$ was employed to analyse the influence of the bias field on polarisation processes by mitigating the overshadowing effect of macroscopic mechanisms (see details in Section 2.2). The raw data of ε' was smoothed with Savitsky-Golay filter since the derivative of the experimental data is sensitive to small deviations. Compared to the original spectrum, the low-frequency slope of $\varepsilon''_{\mathrm{der}}$ drops faster opening up the new relaxation peak 1 (Figure 6.12-b). Two other features (2, 3) can be recognised in $\varepsilon''_{\mathrm{der}}$ at higher frequencies that seem to be independent on the bias field.

The location and magnitude of the peak 1 was analysed by fitting the spectra of $\varepsilon''_{\mathrm{der}}$ with the logarithmic derivative of the Havriliak-Negami function.[30] Figure 6.13 shows the relaxation strength of the peak 1 and frequency of the maximum in dependence of the bias field. The shape of the curve $\Delta\varepsilon(E_{\mathrm{DC}})$ (Figure 6.13-a) matches the shape of the function $\varepsilon''(E_{\mathrm{DC}})$ (Figure 6.4). In $\varepsilon''(E_{\mathrm{DC}})$, measured at a constant frequency, a slight decrease after the plateau was noticed, that was associated with the shift of the peak to higher frequencies (Section 6.2). The shift of the peak 1 is almost linear with the increasing bias field (Figure 6.13-b).

The new relaxation peak is closely related to water in cellulose and occurs at the high frequency side of the β_{wet}-process at room temperature (see Section 4.4.3). Since the MWS, β_{wet} and the peak 1 overlap each other, and the low-frequency end is limited by 5 Hz, it is difficult to conclude how the peak 1 is related to the β_{wet}-peak.

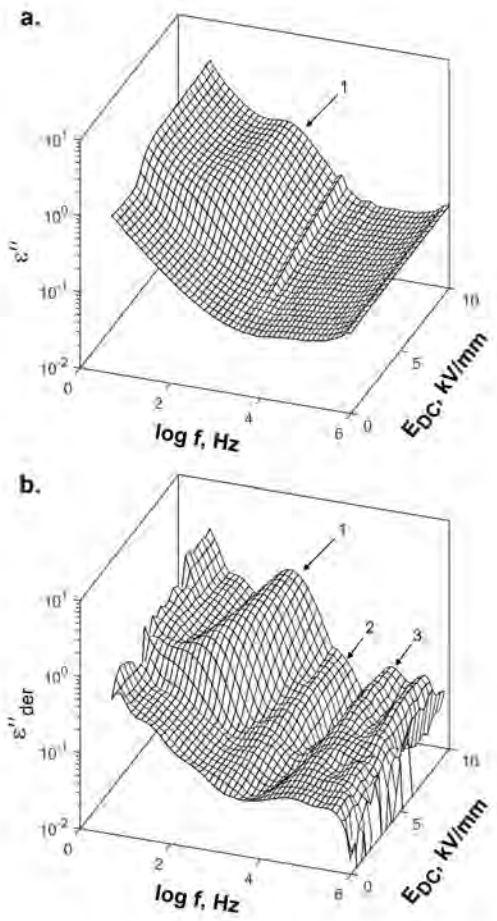

Figure 6.12: Dielectric loss ε'' (a) and logarithmic derivative $-\partial\varepsilon'/\partial\ln\omega$ (b) of a non-impregnated insulating paper Grade K with 7% wt. moisture as function of frequency and the superimposed dc-field.

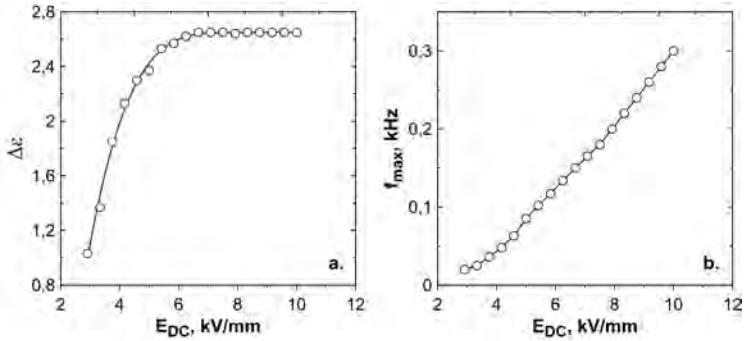

Figure 6.13: The relaxation strength of the peak 1 in Figure 6.12 (a) and the frequency corresponding to the loss peak (b) as functions of the superimposed dc-field.

6.3.2 AC-Conductivity

Ionic transport mechanisms underlying the dc-conductivity and a low-frequency dielectric relaxation in cellulose have been mentioned in Section 4.1. It was noted, that there is a close correlation between the dc-conductivity and a low-frequency dielectric relaxation. The universal shape of conductivity spectra was shown schematically in Figure 4.3. It was mentioned that a knee-like shape in $\sigma'(\omega)$ indicates a local charge transport, that also causes the MWS-relaxation in heterogeneous materials.

Figure 6.14 compares conductivity spectra for various types of electrical contacting, water content and the bias field. In wet specimens, the begin of the transition to the dc-conductivity plateau is visible at the lowest frequencies (curve 1). In contrast, in dried specimens, where the dc-conductivity is much lower, only the linear part of the spectrum was measured (curve 2). Above 100 kHz, the slope of the conductivity increase is greater than 1 which is due to the measurement uncertainty at high frequencies. The conductivity of specimens

contacted with bare electrodes was lower than of silver painted specimens (cf. curves 1 and 5). What has been referred to as the local diffusion that causes an intermediate plateau is visible in curve 4.

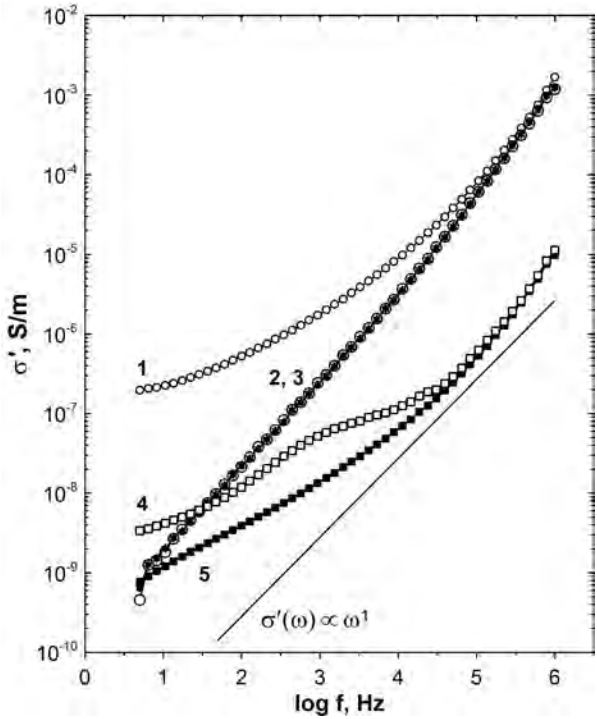

Figure 6.14: Frequency spectra of real part of the complex conductivity of Transformerboard: (1) wet specimen (7 %wt.) contacted with silver paint; (2) dried specimen contacted with silver paint (< 0.5 %wt.) without dc-bias (stars); (3) dried specimen contacted with silver paint (< 0.5 %wt.) at 13 kV/mm$_{DC}$ (circles); (4) wet specimen (7 %wt.) contacted with bare electrodes at 6.75 kV/mm$_{DC}$; (5) wet specimen (7 %wt.) contacted with bare electrodes measured without dc-bias.

6.4 Dielectric Behaviour of the Oil-Impregnated Paper

Comparison of permittivities of air-impregnated and oil-impregnated specimens is shown in Figures 6.15 and 6.16. In presented experiments, the specimens were coated with silver paint prior to dielectric measurements in the air-impregnated state, after which they were impregnated with oil under vacuum. Therewith, the influence of a thin film of oil between the electrodes and paper was eliminated. Introduction of oil into the paper had a greater influence on the real part of the complex permittivity, that was earlier explained by the increase of ε_∞ (cf. Equations **??** and **??**).

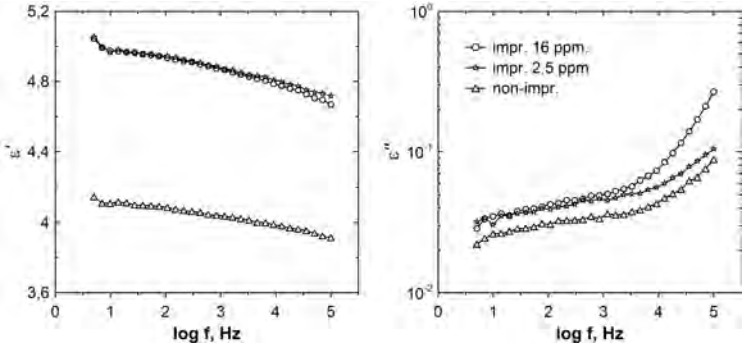

Figure 6.15: Comparison of permittivity spectra of a dry insulating paper with less than 0.5 % wt. water impregnated with air or oil with different water contents at 25°C.

The water content of the oil only slightly affected the increase of the permittivity of paper due to the impregnation. This effect was more pronounced in dry papers impregnated with wet oil (Figure 6.15). The dielectric loss ε'' increased above 1 kHz upon the impregnation with wet oil. ε' and ε'' of wet papers were not significantly affected by the water content of the oil (Figure 6.16).

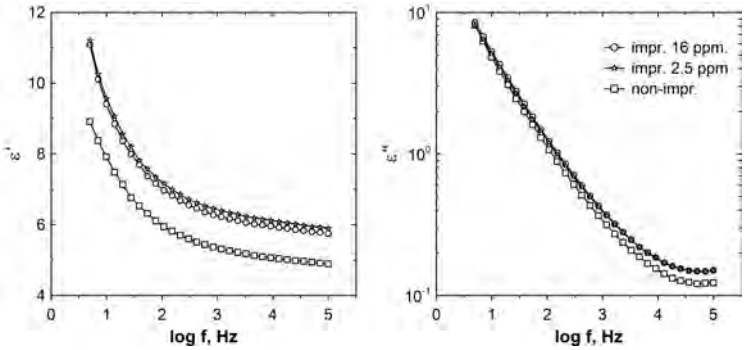

Figure 6.16: Comparison of permittivity spectra of a room-humid insulating paper with 7.8 % wt. water insulated with air or oil with different water contents at 25°C.

6.4.1 Effect of the Bias Field

The complex permittivity of dry paper specimens impregnated with vacuum-dried mineral oil was not affected by a simultaneously applied bias field, similar to what was previously reported for air-impregnated dry specimens. In preliminary tests conducted on specimens with a moderate to high amount of moisture, a significant effect of the electrode-paper interface was identified. For this reason, two types of oil-impregnated specimens were considered in studies involving high bias fields. The impregnated papers were measured without conductive coating. Specimens of the first type were carefully impregnated under vacuum and again subjected to vacuum to remove air inclusions from between the electrodes and paper. Specimens of the second type were similarly impregnated under vacuum but their surfaces were cleared of the excessive oil such that the electrodes were in a closer contact with cellulose fibres. The main difference between the two types of specimens was a thin film of oil separating cellulose fibres from the metal electrodes and filling the surface irregularities of

paper (Figure 5.16-c)

In the specimens of the first type, the permittivity increased only slightly upon the bias field application in comparison to non-impregnated specimens measured under equal conditions (Figure 6.17-a). ε'' increased at lower frequencies, whereas no distinct relaxation peak was found in the intermediate frequency region.

In the second type of specimens where cellulose fibres were in a closer contact with metal electrodes and thus air inclusions were present a relaxation peak occurred in ε'' spectrum similar to what was observed in air-impregnated units (Figure 6.17-b). The maximum of the occurring relaxation peak was observed at lower frequencies than in air-impregnated specimens (cf. Figure 6.10).

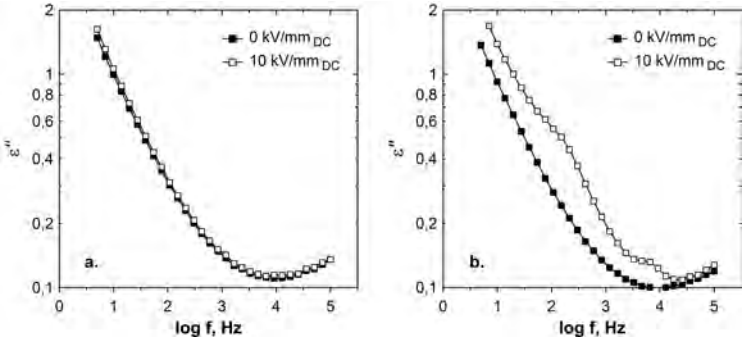

Figure 6.17: Dielectric loss spectra of oil-impregnated insulating papers measured at 25°C. (a) Grade K paper 0.24 mm with 8 % wt. moisture contacted without air inclusions. (b) Grade K paper 0.24 mm with air inclusions at the surface and direct contact of cellulose fibres and metal electrodes.

6.4.2 Properties of a Layered Oil Paper Specimen

The role of the oil film remaining between the metal electrode and paper was further addressed by experiments where a thin oil gap

was subjected to high dc-field and its complex permittivity was measured at the same time. In another experiment, a defined oil gap was created between the paper and the electrode by means of spacers.

The thickness of the oil film was defined by round fused silica spacers placed between the measuring and ground electrodes. To enhance the measured effects, moist oil with 11 ppm water was tested. As shown in Figure 6.18, the high bias field considerably enhanced the dielectric loss at lower frequencies. The increase of the permittivity sustained longer than the permittivity changes in paper even after the removal of the dc-field.

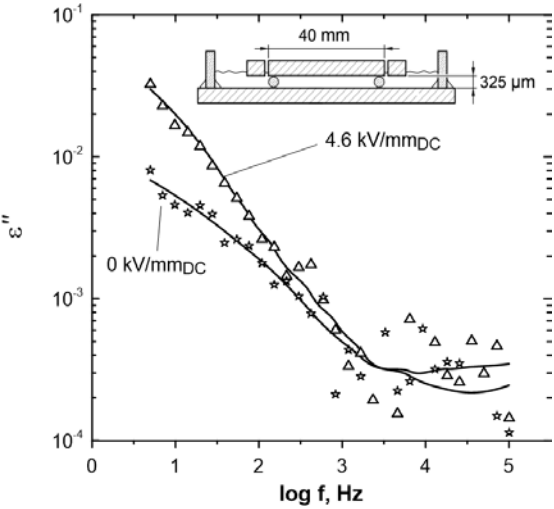

Figure 6.18: Comparison of ε''-spectra of unaged transformer oil with 11 ppm water measured at 24°C with and without bias field application.

The effect of an oil layer separating the electrodes and the paper was studied on a specimen where a little oil gap was created between the paper and electrode by means of 100 µm thin PTFE spacers (Figures 6.19 and 5.13-b). A single layer of Grade K paper of thickness

250 µm in different water contents was placed on the high voltage electrode. The specimens were prepared according to descriptions given in Section 5.2.4. Mineral oil with 11 ppm water was used on purpose.

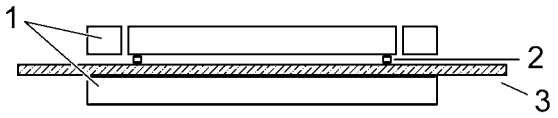

Figure 6.19: Geometry of the two-layer specimen. 1 – metal electrodes, 2 – Teflon spacers, 3 – layer of insulating paper. Thickness of the oil gap 100 µm, thickness of paper 250 µm.

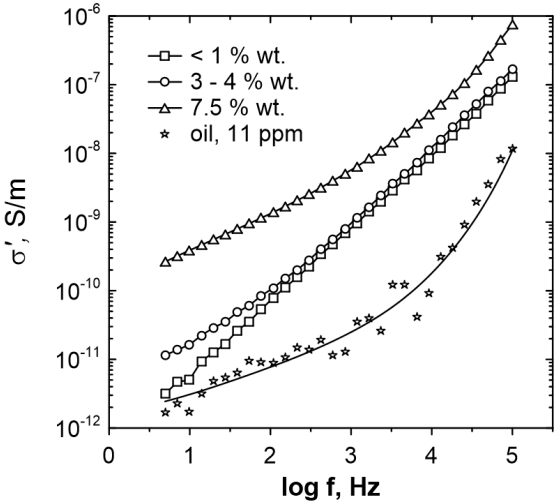

Figure 6.20: Spectra of the real part of the complex conductivity of two-layer specimens and oil measured with an unbiased ac-voltage at 24°C.

The dielectric properties of the paper defined the observed behaviour of the oil-paper layering of given dimensions. The conductivities of the layered specimens at all water contents of the paper were

higher than that of the pure oil (Figure 6.20). σ'-spectra of papers show only the high frequency slope without any sign of the transition to the dc-conductivity plateau. On the other hand, for the oil, the slope of the conductivity spectrum decreases faster. The visual examination suggests that the dc-conductivity of the wet paper containing 7.5 % wt. water is significantly higher than that of the oil with 11 ppm.

The layered arrangement shown in Figure 6.19 and the pure oil gap were subjected to high bias fields. Figure 6.21 plots the absolute changes of ε' and ε'' compared to values measured without the bias field. $\Delta\varepsilon'$ and $\Delta\varepsilon''$ of wet oil thickness is graphed. The permittivity of the oil gap did not increase due to the bias field. In paper-oil system, enhancements ε' and ε'' were higher and depended on the water content of the paper. In the sample with the driest paper, ε' shifted upwards by a constant value while no significant change of ε'' was observed.

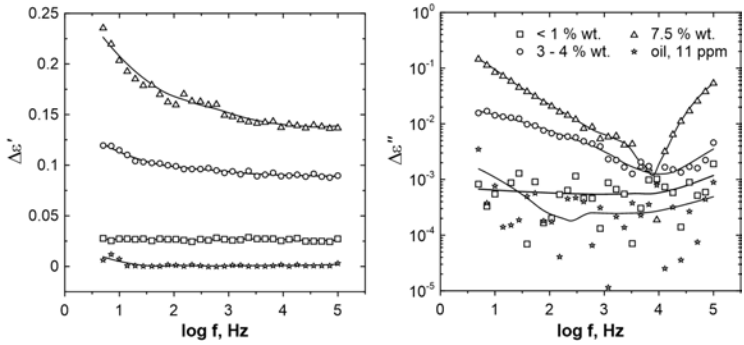

Figure 6.21: Increase of real and imaginary parts of the complex permittivity of a two-layer model (Figure 6.19) and 325 µm thick oil gap due to the application of a bias voltage of 1 kV for different water contents of the paper at 24°C. The water content of oil was constant at 11 ppm.

7 Discussion

7.1 Non-Impregnated Papers

The results have shown that the effect of a superimposed high dc-voltage on the complex permittivity of paper materials is determined by several factors related to the sample preparation and measurement conditions. These factors are discussed below separately although they are closely related to each other and the observed effects were often caused by the combination of several factors.

- **Water content.** Water had the greatest influence on the dielectric behaviour of papers studied in this work. The ways in which water interacts with cellulose and alters its physical properties were described in Section 3.2. In terms of dielectric parameters, the addition of water enhances both ε' and ε'' at low and high frequencies by affecting all known dielectric relaxation mechanisms of cellulose. As for the dc-voltage superposition, the considered papers had to contain a moderate amount of water for their permittivity to be affected by the high bias field. In contrast, the permittivity of thoroughly dried papers did not change. The enhancement of ε' and ε'' due to the high bias field was observed at lower frequencies suggesting that dipolar β and γ relaxation processes, which peaks are located at higher frequencies, remained unaffected. Instead, a peak in the frequency spectrum of ε'' of wet papers resembling a separate relaxation process was measured below several kHz. With the increasing water content the peak shifted to higher frequencies. Cellulose already features a relaxation peak in a similar frequency region known as β_{wet} which is related to hydration. The fact that both the peak observed under the high bias field and β_{wet}-peak are located at similar frequencies and move to higher fre-

quencies with increasing water content could be an indication that similar polarisation mechanisms are responsible for both phenomena. As mentioned earlier, different underlying mechanisms were suggested for the β_{wet} relaxation including proton hopping and molecular motions of cellulose chains in cellulose-water compound. The proton hopping in cellulose and the potential influence of the bias field will be discussed below.

- **Temperature.** The effect of temperature was closely related to the water content of the paper. In dried papers, at a high temperature, the bias field had almost no effect on both parts of the complex permittivity. On the other hand, ε' and ε'' of wet papers increased more significantly with the bias field when warmed up. The water content of the paper is sensitive even to small changes of temperature. Therefore, the observed changes of the permittivity were likely due to not only the bias field but also due to the decreasing water content. In other words, the enhancing effect of the bias field on ε' and ε'' was partly compensated by the gradual decrease of the water content.
- **Frequency and amplitude of the sensing ac-voltage.** ε' and ε'' were influenced by the bias field at frequencies below several kHz depending on the water content. Increasing the amplitude of the sensing ac-voltage limited the effect of the bias field on ε' and ε''.
- **Electrical contacting.** The way the paper sample was contacted with solid electrodes had a significant effect on results. At low-voltages, by coating the paper with a conductive layer, higher values of ε' and ε'' in contrast to bare metal electrodes were measured. The microscopic air gaps lower the permittivity by acting like series capacitances. In measurements with high dc-voltages, the electrical contacting affected the permittivities of

wet papers but had no influence on dry papers. In fact the effect of the bias field on wet papers in form of a relaxation peak was only noticed in papers contacted with bare metal electrodes. Only slight changes in ε' and ε'' were measured when using conductive silver paint. This observation indicates that high local electric fields at the metal-paper interface in combination with a relatively high water content are necessary to influence the permittivity when subjecting to high bias fields.

The role of high electric fields and water content on the permittivity can be interpreted as follows. It is assumed that the observed changes of the permittivity are due to ionic relaxation processes. This assumption is made solely on the basis of the visual examination of the dielectric spectra, particularly on the fact that the slopes in ε''-spectrum at higher frequencies ascribed to dipolar relaxation processes remained unaffected when subjecting to high bias fields.

As suggested by other authors, water, on the one hand, increases the number of mobile ions by adding protons and other ionic species. On the other hand, it facilitates ionic motions by building conductive paths. When applying a high bias field, the local field hotspots at surface irregularities of the paper are likely to cause the electrochemical decomposition of water molecules. As a result, the concentration of mobile ions is increased.

The occurrence of a relaxation peak in the ε''-spectrum under the influence of the high bias field is likely due to the hopping motions of ions generated by high electric fields. The probability of hopping transitions increases of ions depends on the water content of the paper. The higher the water content, the more available sites has the ion to move to from its current site under the influence of a bias field. The hopping probability also increases with the height of the bias field. The higher the probability of hopping transitions, the higher is the

frequency of the corresponding relaxation peak as was mentioned in section 4.1.

To interpret the effect of the amplitude of the sensing ac-voltage a model of potential barriers is suggested. The ionic migration in solids is determined by the distribution of potential barriers. In a disordered system like cellulose, the potential barrier landscape can be imagined as a "basin" with a corrugated bottom (Figure 7.1). The ions can move within areas of relatively low barriers by surmounting them under the influence of the applied electric field. However, higher barriers restrict the ionic motions and do not allow the ions to leave the "basin". This leads to a charge separation on both sides of a high barrier and is detected dielectrically as an increase of the complex permittivity since separated charges act as dipoles. It is assumed that superimposing a similarly high ac voltage of a sufficiently low frequency to the dc-bias increases the probability of transitions over higher barriers due to much higher combined electric field, allowing the ions to distribute more evenly. Less local charge concentrations can appear in this case, which presumably elucidates the observed limited increase of the permittivity. However, even at higher ac-voltages a substantial increase of the permittivity at the lowest frequencies was noticed, which might be due to longer ranges of motions and greater dipole moments typical for the Maxwell-Magner-Sillars-relaxation.

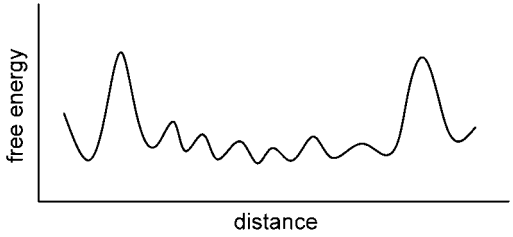

Figure 7.1: Potential barrier distribution.

7.2 Oil-Impregnated Papers

Although the complex permittivity of an oil-impregnated paper is dominated by dielectric relaxation processes in cellulose, the presence of oil in paper makes it to a more complex mixed dielectric than in the air-impregnated state. The results show, that the complex permittivity of a well-dried paper and oil combined to a void-free dielectric is not affected by a strong bias field, at least not in the considered range of frequencies and temperatures. Only if the electric field was high enough at the surface of the paper, did a distinct relaxation peak occur, similar to what was seen in air-impregnated papers. Therefore, it is assumed that also in oil-impregnated specimens, the electrical decomposition of water adsorbed in cellulose is the main mechanism explaining the emergence of a loss peak when applying a high bias field. The interfacial polarisation peak due to differently conductive oil and cellulose fibres seems to arise at lower frequencies, which were not observed in this study. The decrease of the dielectric loss due to the bias field, that was reported by other authors as the cause of ionic depletion, could not be observed in considered specimens. At the same time, measurements of the complex permittivity under the application of a bias field identified a complex set of dielectric phenomena taking place at solid-liquid boundaries. The results suggest that under the influence of the high bias field space charge is formed, whereas mobile ions of both oil and paper are involved. Understanding the relationship between the space charge accumulation in a static electric field and the associated increase of the permittivity of the oil-impregnated paper requires further investigations.

7.3 Application in Medium-Frequency Transformers

The complex permittivity of well-dried insulating papers unaffected by a high bias field indicate that the molecular motions of cel-

lulose chains are not influenced by the bias fields of considered magnitudes. This is in conformity with the idea that the externally applied electric field is not equal to the local field acting upon dipoles. The latter is significantly distorted by dipolar interactions. Therewith, only ionic polarisation mechanisms seem to be influenced by the bias field.

The PWM voltage with a fast slew rate used in medium frequency transformers features a high harmonic content that depends on the rise time of pulses and their repetition frequency. Under the influence of such electric stress, each frequency component contributes to the total dielectric loss an amount proportional to frequency, the corresponding dielectric loss factor and the square of the voltage

$$P_{\text{diel.}} = \frac{1}{2} U_0^2 \omega \varepsilon''(\omega) C_0 \,, \tag{7.1}$$

where $U = U_0 \sin(\omega t)$ is the sinusoidal voltage applied to a dielectric enclosed into a capacitor of geometric capacitance C_0. The total dielectric loss is determined as the sum of contributions of Fourier components of the applied multifrequency voltage

$$P_\Sigma = \frac{1}{2} \sum_{n=1}^{\infty} U_{0,n}^2 \omega_n \varepsilon''(\omega_n) C_0 \,. \tag{7.2}$$

Hence the dielectric heating is an important factor to consider in MFTs, if the electric stress features high frequency components of high amplitude.[9–11] The total dielectric loss cannot be estimated from ε'' that is known only for one frequency, e. g. 50 Hz. As seen in Figure 7.2, due to fast dipolar relaxation mechanisms of cellulose, ε'' of dry cellulose increases with the increasing frequency. As for the use of cellulosic papers in medium-frequency transformers, a greater dielectric loss is to be expected in the insulation than in low-frequency applications. Firstly, it is associated with the higher frequency. Secondly,

the dielectric loss factor of cellulose increases towards higher frequencies. Considering both factors together, the loss calculated according to Equation 7.2 can be anticipated to become larger than at 50 Hz. Based on the results of the present work, it can also be stated that the amount of the dielectric loss is not influenced by a simultaneously acting high bias field. Thoroughly dried cellulosic insulating papers exhibit dielectric losses not much higher than synthetic fibrous materials. However, the maintenance of a high degree of dryness of cellulosic papers in oil-immersed medium-frequency transformers is imperative to ensure low dielectric losses and to avoid detrimental effects of water on the paper insulation.

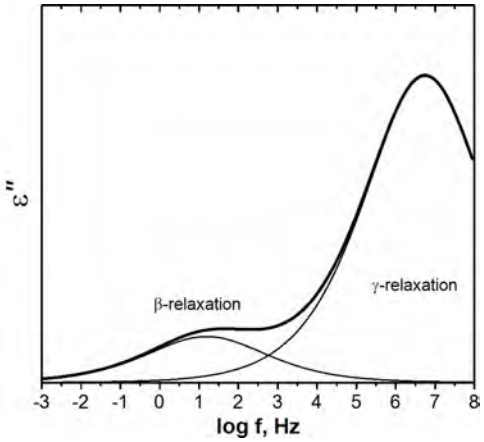

Figure 7.2: Schematic of the loss spectrum of dry cellulose with indication of relaxation processes at temperatures around room temperature.

8 Summary and Outlook

Within the scope of the present work an experimental effort was undertaken with the intention to characterise the dielectric relaxation phenomena in cellulosic insulating papers, subjected to high mixed electric fields. Detailed conclusions can be found at the ends of corresponding sections as well as in the discussion.

The unique properties of cellulose, especially in the interaction with water, make it a remarkably complex material. At the same time, it can be considered as an insightful model substance. The results of experiments involving high bias fields suggest that proton migration determines the origin of the relaxation mechanism in cellulose associated with its hydration. The increase of proton concentration due to the ionisation at the surface of paper specimens is assumed to cause an additional dielectric relaxation in the intermediate frequency region with a loss peak arising at several hundred hertz at room temperature. A model of random potential barriers was employed to elucidate the origin of the arising relaxation.

As revealed in presented experiments, dielectric properties of insulating papers in an unaged state were unaffected by the presence of a high static field. It was only at higher degrees of ageing accompanied with an increase of the water content of cellulose and at improper electrical contacting, where a high dc-field enhanced the complex permittivity. The enhancement of dielectric properties in a relatively wide range of frequencies, i. e. up to 100 kilohertz may be associated with a substantial increase of dielectric losses. However, the higher degrees of hydration which were considered in the work were rather exaggerated. These water contents would be a sign for severe deterioration of the insulation of a real apparatus. The proper drying and avoidance of gas-filled inclusions are well-known prerequisites for the reliable

operation of the oil-impregnated insulation. Their importance was underlined by the presented experimental evidence. The sensitivity of dielectric losses in the cellulosic paper to water content and temperature could become a limiting factor for the use in medium-frequency medium-voltage transformers with high requirements on thermal and electrical properties of dielectric materials. However, further specific investigations including different insulating materials are needed to give a more exhaustive conclusion.

Improvements of experimental facilities combined with a research in listed directions would supplement and verify the observations presented in this work:

- Extension of the frequency range towards lower frequencies would provide valuable information concerning the macroscopic relaxation processes in terms of the complex permittivity and the complex conductivity.
- Extension of measurement temperatures to lower degrees would be particularly important in the observation of phenomena related to hydration, since the water content of cellulose starts to decrease at around 50°C. Lower temperatures are also reasonable for the investigation of secondary relaxation mechanisms due to the shift of the secondary loss peaks to lower frequencies.
- Application of dielectric spectroscopy at higher magnitudes of the probing ac-voltage would be another insightful way of extending the knowledge obtained from low-field measurements, especially in addressing the processes due to ionic motions.

References

[1] J. Thoma, S. Kolb, C. Salzmann, and D. Kranzer. Characterization of high-voltage-sic-devices with 15 kv blocking voltage. In *2016 IEEE International Power Electronics and Motion Control Conference (PEMC)*, pages 946–951, 2016.

[2] A. Q. Huang. Medium-voltage solid-state transformer: Technology for a smarter and resilient grid. *IEEE Industrial Electronics Magazine*, 10(3):29–42, 2016.

[3] D. Schröder and R. Marquardt. *Leistungselektronische Schaltungen: Funktion, Auslegung und Anwendung*. Springer Berlin Heidelberg, 2018.

[4] C. Zhao, D. Dujic, A. Mester, J. K. Steinke, M. Weiss, S. Lewdeni-Schmid, T. Chaudhuri, and P. Stefanutti. Power electronic traction transformer—medium voltage prototype. *IEEE Transactions on Industrial Electronics*, 61(7):3257–3268, 2014.

[5] S. Candolfi, S. Blume, D. Aguglia, P. Viarouge, J. Biela, and J. Cros. Evaluation of insulation systems for the optimal design of high voltage pulse transformers. In *2014 IEEE International Power Modulator and High Voltage Conference (IPMHVC)*, pages 557–560, 2014.

[6] T. Guillod. *Modeling and Design of Medium-Frequency Transformers for Future Medium-Voltage Power Electronics Interfaces*. PhD thesis, ETH Zurich, Zurich, 2018.

[7] R. Färber. *Endurance of Polymeric Insulation under Mixed-Frequency Medium-Voltage Stress*. PhD thesis, ETH Zurich, Zurich, 2019.

[8] J. C. G. Wheeler. Effects of converter pulses on the electrical insulation in low and medium voltage motors. *IEEE Electrical Insulation Magazine*, 21(2):22–29, 2005.

[9] B. Sonerud, T. Bengtsson, J. Blennow, and S. M. Gubanski. Dielectric heating in insulating materials subjected to voltage waveforms with high harmonic content. *IEEE Transactions on Dielectrics and Electrical Insulation*, 16, 2009.

[10] M. Birle and C. Leu. Dielectric heating in insulating materials at high dc and ac voltages superimposed by high frequency high voltages. 2013.

[11] T. Guillod, R. Färber, F. Krismer, C. M. Franck, and J. W. Kolar. Computation and analysis of dielectric losses in mv power electronic converter insulation. In *2016 IEEE Energy Conversion Congress and Exposition (ECCE)*, pages 1–8, Sep. 2016.

[12] R. Richert. *Nonlinear Dielectric Spectroscopy*. Advances in Dielectrics. Springer International Publishing, 2018.

[13] J. Małecki. Non-linear dielectric behaviour and chemical equilibria in liquids. *Electrochimica Acta*, 33(9):1235 – 1241, 1988.

[14] C.J.F. Böttcher. *Theory of electric polarization: Dielectrics in static fields*. Number Bd. 1. Elsevier, 1973.

[15] R. Richert. Nonlinear dielectric effects in liquids: A guided tour. *Journal of Physics Condensed Matter*, 29(36), 8 2017.

[16] H. Block and E. F. Hayes. Dielectric behaviour of stiff polymers in solution when subjected to high voltage gradients. *Trans. Faraday Soc.*, 66:2512–2525, 1970.

[17] C. G. Garton. Dielectric loss in thin films of insulating liquids. *Journal of the Institution of Electrical Engineers - Part II: Power Engineering*, 88(2):103–120, April 1941.

[18] F. Liebscher and W. Held. *Kondensatoren: Dielektrikum Bemessung Anwendung*. Springer Berlin Heidelberg, 1968.

[19] S. Osaki, S. Uemura, and Y. Ishida. Effects of a static electric field upon dielectric properties of poly(vinylidene fluoride) and poly(vinyl fluoride). *Journal of Polymer Science Part A-2: Polymer Physics*, 9(4):585–594, 1971.

[20] S. Uemura. Ionic contribution to the complex dielectric constant of a polymer under dc bias. *Journal of Polymer Science: Polymer Physics Edition*, 10(11):2155–2166, 1972.

[21] G. S. Kuchinsky. Measurement of loss tangent under simultaneous action of d.c. and a.c. voltages. *Elektrichestvo*, (6):52–54, 1952.

[22] G. S. Kuchinsky. The behaviour of paper-oil insulation under a.c. voltage with simultaneous d.c. component. *Elektrichestvo*, (10):45–49, 1955.

[23] D. H. Hogle, M. M. Rutter, and T. W. Dakin. Dielectric properties of cyanoethylcellulose. In *1957 Conference on Electrical Insulation*, pages 51–52, 1957.

[24] Z. Krasucki, H. F. Church, and C. G. Garton. A new explanation of gas evolution in electrically stressed oil-impregnated paper insulation. *Journal of The Electrochemical Society*, 107(7):598, 1960.

[25] C. G. Garton Z. Krasucki, H. F. Church. *Factors controlling the life of power capacitors. Cigre-Report N. 138.* 1962.

[26] M. Rapos. The electrical properties of insulating materials under the simultaneous action of ac and dc voltage. In *Conference on Electrical Insulation Dielectric Phenomena - Annual Report 1972*, pages 98–104, Oct 1972.

[27] W. Taschner. *Öl- und Ölpapier bei Gleich- und Wechselspannung insbesondere bei Überlagerung beider Spannungsarten*. PhD thesis, TU Darmstadt, Darmstadt, 1972.

[28] H. Shimokawa, A. Ohashi, and M. Ueda. Voltage dependence of tan δ of dielectric liquid films. *Electrical Engineering in Japan*, 101(1):14–20, 1981.

[29] A.K. Jonscher. *Dielectric Relaxation in Solids*. Chelsea Dielectrics Press Limited, 1983.

[30] M. Wübbenhorst and J. v. Turnhout. Analysis of complex dielectric spectra. i. one-dimensional derivative techniques and three-dimensional modelling. *Journal of Non-Crystalline Solids*, 305(1):40 – 49, 2002.

[31] P.A.M. Steeman. *Interfacial phenomena in polymer systems: A dielectric approach*. Doctoral Thesis. TU Delft, 1992.

[32] M. Dochia, C. Sirghie, R.M. Kozłowski, and Z. Roskwitalski. 2 - cotton fibres. In R. M. Kozłowski, editor, *Handbook of Natural Fibres*, volume 1 of *Woodhead Publishing Series in Textiles*, pages 11 – 23. Woodhead Publishing, 2012.

[33] T. A. Prevost and T. V. Oommen. Cellulose insulation in oil-filled power transformers: Part i - history and development. *IEEE Electrical Insulation Magazine*, 22(1):28–35, Jan 2006.

[34] H. Gasser, C. Krause, and T. Prevost. Water absorption of cellulosic insulating materials used in power transformers. In *2007 IEEE International Conference on Solid Dielectrics*, pages 289–293, July 2007.

[35] E. Westhof. *Water and Biological Macromolecules*. Topics in Molecular and Structural Biology. Macmillan Education UK, 1993.

[36] T. Hatakeyama and H. Hatakeyama. *Thermal Properties of Green Polymers and Biocomposites*. Hot Topics in Thermal Analysis and Calorimetry. Springer Netherlands, 2004.

[37] E. L. Lindh and L. Salmén. Surface accessibility of cellulose fibrils studied by hydrogen–deuterium exchange with water. *Cellulose*, 24(1):21–33, Jan 2017.

[38] K. Nakamura, T. Hatakeyama, and H. Hatakeyama. Studies on bound water of cellulose by differential scanning calorimetry. *Textile Research Journal*, 51(9):607–613, 1981.

[39] T. V. Oommen. Moisture equilibrium charts for transformer insulation drying practice. *IEEE Transactions on Power Apparatus and Systems*, PAS-103(10):3062–3067, Oct 1984.

[40] E.J. Murphy. The dependence of the conductivity of cellulose, silk and wool on their water content. *Journal of Physics and Chemistry of Solids*, 16(1):115 – 122, 1960.

[41] M. Nilsson and M. Strømme. Electrodynamic investigations of conduction processes in humid microcrystalline cellulose tablets. *The Journal of Physical Chemistry B*, 109(12):5450–5455, 2005. PMID: 16851580.

[42] J F Nagle and H J Morowitz. Molecular mechanisms for proton transport in membranes. *Proceedings of the National Academy of Sciences*, 75(1):298–302, 1978.

[43] H. E. Taylor. The dielectric relaxation spectrum of glass. *Trans. Faraday Soc.*, 52:873–881, 1956.

[44] T. Nakajima. Correlation between electrical conduction and dielectric polarization in inorganic glasses. In *Conference on Electrical Insulation Dielectric Phenomena - Annual Report 1971*, pages 168–176, 1971.

[45] H. Namikawa. Characterization of the diffusion process in oxide glasses based on the correlation between electric conduction and dielectric relaxation. *Journal of Non-Crystalline Solids*, 18(2):173 – 195, 1975.

[46] J. C. Dyre and T. B. Schrøder. Universality of ac conduction in disordered solids. *Rev. Mod. Phys.*, 72:873–892, Jul 2000.

[47] J. Einfeldt, D. Meißner, and A. Kwasniewski. Contributions to the molecular origin of the dielectric relaxation processes in polysaccharides – the high temperature range. *Journal of Non-Crystalline Solids*, 320(1):40 – 55, 2003.

[48] P. Ortiz-Serna, M. Carsí, B. Redondo-Foj, and M.J. Sanchis. Electrical conductivity of natural rubber–cellulose ii nanocomposites. *Journal of Non-Crystalline Solids*, 405:180 – 187, 2014.

[49] R. J. Charles. Some structural and electrical properties of lithium silicate glasses. *Journal of the American Ceramic Society*, 46(5):235–238, 1963.

[50] P. Hedvig. *Dielectric spectroscopy of polymers*. Wiley, 1977.

[51] J. Heijboer. Secondary loss peaks in glassy amorphous polymers. *International Journal of Polymeric Materials and Polymeric Biomaterials*, 6(1-2):11–37, 1977.

[52] J. Kolařík. Secondary relaxations in glassy polymers: Hydrophilic polymethacrylates and polyacrylates. In *Behavior of Macromolecules*, pages 119–161, Berlin, Heidelberg, 1982. Springer Berlin Heidelberg.

[53] S. Cerveny, J. Colmenero, and Á. Alegría. Dielectric properties of water in amorphous mixtures of polymers and other glass forming materials. *Journal of Non-Crystalline Solids*, 353(47):4523 – 4527, 2007. Dielectric Relaxation and Related Phenomena.

[54] J. Kolařík and J. Janáček. Effect of low molecular weight compounds on the relaxation behavior of poly(2-hydroxyethyl methacrylate) in the glassy state and in the transition region from the glassy to the rubberlike state. *Journal of Polymer Science Part A-2: Polymer Physics*, 10(1):11–22, 1972.

[55] J. Einfeldt, D. Meißner, and A. Kwasniewski. Comparison of the molecular dynamics of celluloses and related polysaccharides in wet and dried states by means of dielectric spectroscopy. *Macromolecular Chemistry and Physics*, 201(15):1969–1975, 2000.

[56] Derek J. Crofton and Richard A. Pethrick. Dielectric studies of proton migration and relaxation in wet cellulose and its derivatives. *Polymer*, 22(8):1048 – 1053, 1981.

[57] G. Jafarpour, F. Roig, E. Dantras, A. Boudet, and C. Lacabanne. Influence of water on localized and delocalized molecular mobility of cellulose. *Journal of Non-Crystalline Solids*, 355(34):1669 – 1672, 2009.

[58] H. Montes, J.Y. Cavaillé, and K. Mazeau. Secondary relaxations in amorphous cellulose. *Journal of Non-Crystalline Solids*, 172-174:990 – 995, 1994. Proceedings of the Second Internatinal Discussion Meeting on Relaxations in Complex Systems.

[59] K. Kaminski, E. Kaminska, K. L. Ngai, M. Paluch, P. Wlodarczyk, A. Kasprzycka, and W. Szeja. Identifying the origins of two secondary relaxations in polysaccharides. *The Journal of Physical Chemistry B*, 113(30):10088–10096, 2009.

[60] G. P. Johari and M. Goldstein. Viscous liquids and the glass transition. ii. secondary relaxations in glasses of rigid molecules. *The Journal of Chemical Physics*, 53(6):2372–2388, 1970.

[61] K. Kaminski, K. Adrjanowicz, D. Zakowiecki, E. Kaminska, P. Wlodarczyk, M. Paluch, J. Pilch, and M. Tarnacka. Dielectric studies on molecular dynamics of two important disaccharides: Sucrose and trehalose. *Molecular Pharmaceutics*, 9(6):1559–1569, 2012.

[62] F. Khan and N. Pilpel. An investigation of moisture sorption in microcrystalline cellulose using sorption isotherms and dielectric response. *Powder Technology*, 50(3):237 – 241, 1987.

[63] J. Einfeldt, D. Meißner, and A. Kwasniewski. Polymerdynamics of cellulose and other polysaccharides in solid state-secondary dielectric relaxation processes. *Progress in Polymer Science*, 26(9):1419 – 1472, 2001.

[64] Ya. Ryabov, A. Gutina, V. Arkhipov, and Yu. Feldman. Dielectric relaxation of water absorbed in porous glass. *The Journal of Physical Chemistry B*, 105(9):1845–1850, 03 2001.

[65] K. Yamamoto and H. Namikawa. Conduction current relaxation of inhomogeneous conductor i. *Japanese Journal of Applied Physics*, 27(Part 1, No. 10):1845–1851, oct 1988.

[66] M. Chang. Folding chain model and annealing of cellulose. *Journal of Polymer Science Part C: Polymer Symposia*, 36(1):343–362, 1971.

[67] J. M. B. Fernandes Diniz, M. H. Gil, and J. A. A. M. Castro. Hornification—its origin and interpretation in wood pulps. *Wood Science and Technology*, 37(6):489–494, 2004.

[68] R. Richert. A simple current-to-voltage interface for dielectric relaxation measurements in the range 1 mhz to 10 mhz. *Review of Scientific Instruments*, 67(9):3217–3221, 1996.

[69] New integrated dielectric analyzer extends accuracy and impedance range for material measurements. *Dielectric Newsletter. Novocontrol*.

[70] *Electrical insulating papers.* WEIDMANN Electrical AG.

[71] *Transformerboard. Cellulosic insulation of unsurpassed quality.* WEIDMANN Electrical AG.

[72] F. Liebscher. Über die dielektrischen Verluste und die Kurvenform der Ströme in geschichteten Isolierstoffen bei hohen Wechselfeldstärken von 50 hz. *Wiss. Veröff. a. d. Siemens-Werken*, 12:214–248, 1943.

[73] E. Scholz. *Karl-Fischer-Titration: Methoden zur Wasserbestimmung*. Anleitungen für die chemische Laboratoriumspraxis. Springer Berlin Heidelberg, 2013.

[74] IEC 60554-2. cellulosic papers for electrical purposes - Part 2: Methods of test, November 2001.

[75] A. Rachocki, E. Markiewicz, and Jadwiga Tritt-Goc. Dielectric relaxation in cellulose and its derivatives. *Acta Physica Polonica A - ACTA PHYS POL A*, 108, 01 2006.

[76] I Semenov and C. Leu. Effect of high dc field on loss tangent and permittivity of non-impregnated transformer board. In Bálint Németh, editor, *Proceedings of the 21st International Symposium on High Voltage Engineering*, pages 336–346, Cham, 2020. Springer International Publishing.

Acknowledgement

I express my deepest gratitude to: my supervisor Dr. Carsten Leu for making this project possible, for his advice and encouragement throughout the work; my colleagues in the research unit High-Voltage Technologies at TU Ilmenau for excellent feedback and support over the years; WEIDMANN Electrical AG for the financial support and providing sample materials and valuable information; Prof. Klaus Heinemann of TITK Rudolstadt for helpful advice on many questions; Dr. Andrea Knauer for making beautiful micrographs; Dr. Thomas Stauden for helping me in building the test facilities; Dr. Raphael Färber of ETH Zurich for valuable discussions; my family and friends for their continued support and friendship.